Tip optofluidic immunoassay: Evaluating COVID-19 antibody protection with 1 μL fingertip blood

Xiaotian Tan*,#, Yujuan Chai*,#, Ruihan Li#, Binmao Zhang#, Hao Li#, Jie Zhang, Tianen Zhu, Weishu Wu, Lixiang An, Shi Hu, Bin Yang, Li Wang, Zhenqiu Cao, Hongjiu Zhang, Peng Wang, Lingling Yu, Shan Yin, Xingyu Li, Fei Shao, Jianheng Huang, Jinze Li, Fan Yang, Chao Zhao, Jiajia Guo, Lin Zeng, Dong Liang, Zhengting Zou, Hairong Zheng*, Xudong Fan*, Liangzhi Xie*, Yunlong Cao*, Hui Yang*

#These authors contributed equally to this work
*Correspondence: xt.tan@siat.ac.cn (X.T.); chaiyj@szu.edu.cn (Y.C.); hr.zheng@siat.ac.cn (H.Z.); xsfan@umich.edu (X.F.); LX@sinocelltech.com (L.X.); yunlongcao@pku.edu.cn (Y.C.); hui.yang@siat.ac.cn (H.Y.)
Received: February 7, 2025; Revised: April 10, 2025; Accepted: April 13, 2025
Doi:10.1016/j.hlife.2025.04.005

Citation: Tan X, Chai Y, Li R, et al. Tip optofluidic immunoassay: Evaluating COVID-19 antibody protection with 1 μL fingertip blood. *hLife* 2025;3:338–356.

GRAPHICAL ABSTRACT

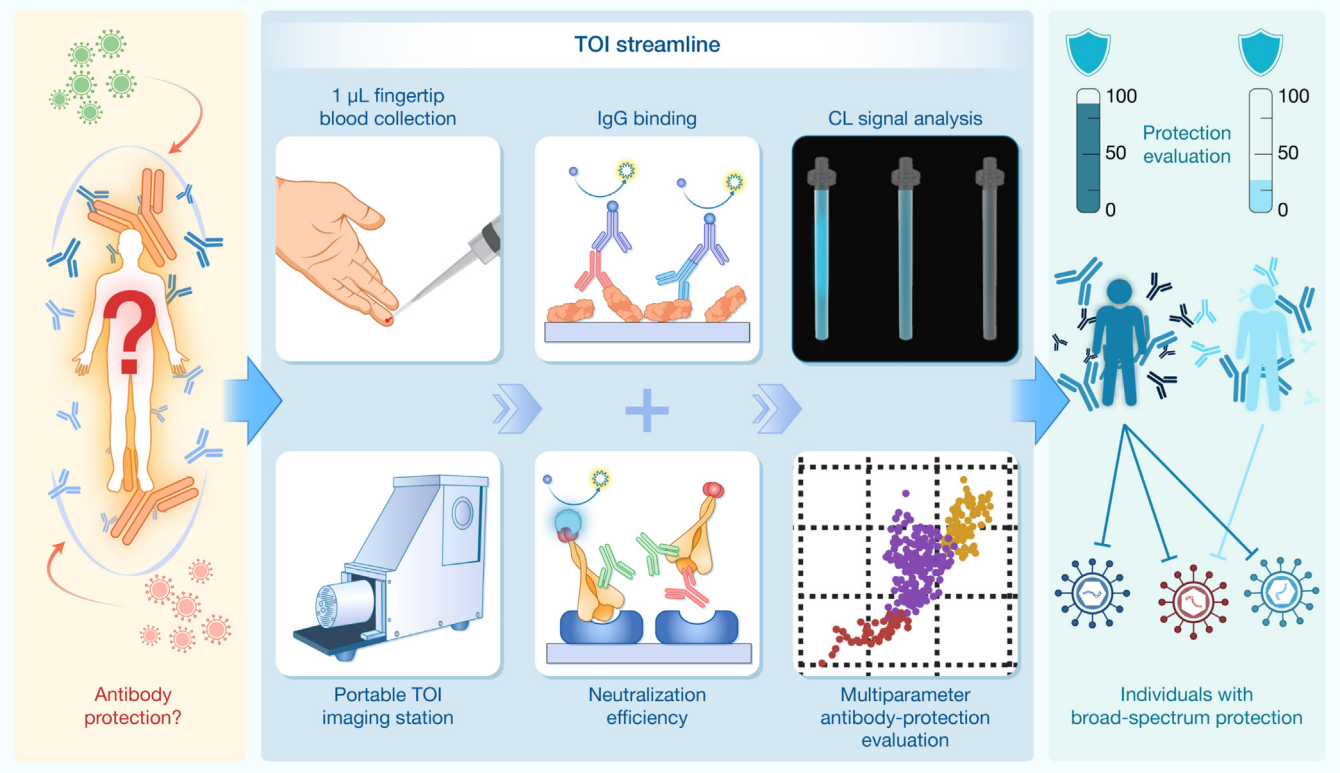

HIGHLIGHTS

- **Multimodal COVID-19 antibody protection evaluation with tip optofluidic immunoassay: binding, kinetics, and neutralization.**
- **Requires only 1 μL of fingertip blood, delivers full results in 40 min; rapid and patient-friendly.**
- **Lower limit of detection of 0.1 ng/mL, 3–4 log dynamic range, signal-to-noise ratio ~10,000; ensures high precision and sensitivity.**
- **Identified 4 volunteers with broad-spectrum antibody protection against two strains of SARS-CoV-2.**

Tip optofluidic immunoassay: Evaluating COVID-19 antibody protection with 1 μL fingertip blood

Xiaotian Tan[1,2,*,#], Yujuan Chai[3,*,#], Ruihan Li[1,2,#], Binmao Zhang[1,3,#], Hao Li[1,4,#], Jie Zhang[5], Tianen Zhu[6], Weishu Wu[7], Lixiang An[4], Shi Hu[1,2,8], Bin Yang[5], Li Wang[5], Zhenqiu Cao[9], Hongjiu Zhang[9], Peng Wang[10], Lingling Yu[10], Shan Yin[10], Xingyu Li[10], Fei Shao[10], Jianheng Huang[1,3], Jinze Li[1], Fan Yang[2,11], Chao Zhao[1,2], Jiajia Guo[1,2], Lin Zeng[1,2], Dong Liang[1,2], Zhengting Zou[9], Hairong Zheng[1,2,*], Xudong Fan[7,*], Liangzhi Xie[5,12,13,*], Yunlong Cao[10,14,*], Hui Yang[1,2,*]

[1]Institute of Biomedical and Health Engineering, Shenzhen Institutes of Advanced Technology, Chinese Academy of Sciences, Guangdong, China
[2]State Key Laboratory of Biomedical Imaging Science and System, Guangdong, China
[3]Department of Biomedical Engineering, Shenzhen University Medical School, Shenzhen University, Guangdong, China
[4]National Innovation Center for Advanced Medical Devices, Guangdong, China
[5]Beijing Key Laboratory of Monoclonal Antibody Research and Development, Sino Biological Inc., Beijing, China
[6]Emergency Department, Shenzhen University General Hospital, Shenzhen University, Guangdong, China
[7]Department of Biomedical Engineering, University of Michigan, Michigan, USA
[8]University of Chinese Academy of Sciences, Beijing, China
[9]Institute of Zoology, Chinese Academy of Sciences, Beijing, China
[10]Changping Laboratory, Beijing, China
[11]Institute of Biomedicine and Biotechnology, Shenzhen Institutes of Advanced Technology, Chinese Academy of Sciences, Guangdong, China
[12]Beijing Engineering Research Center of Protein and Antibody, Sinocelltech Ltd., Beijing, China
[13]Cell Culture Engineering Center, Chinese Academy of Medical Sciences & Peking Union Medical College, Beijing, China
[14]BIOPIC, Peking University, Beijing, China
[#]These authors contributed equally to this work
*Correspondence: xt.tan@siat.ac.cn (X.T.); chaiyj@szu.edu.cn (Y.C.); hr.zheng@siat.ac.cn (H.Z.); xsfan@umich.edu (X.F.); LX@sinocelltech.com (L.X.); yunlongcao@pku.edu.cn (Y.C.); hui.yang@siat.ac.cn (H.Y.)
Received: February 7, 2025; Revised: April 10, 2025; Accepted: April 13, 2025
Doi:10.1016/j.hlife.2025.04.005

Citation: Tan X, Chai Y, Li R, et al. Tip optofluidic immunoassay: Evaluating COVID-19 antibody protection with 1 μL fingertip blood. *hLife* 2025;3:338–356.

ABSTRACT

Infectious diseases such as coronavirus disease 2019 (COVID-19) continue to pose significant global health challenges. Effective management of reinfection risks depends on sustained levels of binding and neutralizing antibodies. However, conventional methods—such as enzyme-linked immunosorbent assays (ELISA) and virus neutralization tests (VNT)—are limited by complex workflows, long assay durations, and high sample volume requirements, making them less suitable for routine, decentralized, or time-sensitive surveillance. This study presents a custom-developed tip optofluidic immunoassay (TOI) platform that enables rapid, multiplexed antibody profiling using only 1 μL of fingertip blood. The system integrates batch-fabricated microfluidic immunoreactors with a portable chemiluminescent imaging station, completing both binding and neutralization capability assessments within 40 min. TOI achieves a broad dynamic range (3–4 orders of magnitude), high signal-to-noise ratio (~10,000), and excellent sensitivity for immunoglobulin G (IgG) detection. A renovated version of the rapid *in vitro* inhibition assay (RIVIA) is incorporated to evaluate neutralizing antibodies against severe acute respiratory syndrome coronavirus 2 (SARS-CoV-2) with greater speed and cost-efficiency. In clinical studies, TOI successfully quantified antibody protection against multiple variants, identifying individuals with broad-spectrum immunity to both wild-type and XBB strains. With its high-precision, rapid turnaround, and minimal sample requirement, TOI offers a valuable tool for decentralized immune surveillance and personalized immunization strategy development.

KEYWORDS fingertip blood; optofluidic immunoassay; antibody protection assessment; coronavirus disease 2019 (COVID-19); biosensing

INTRODUCTION

Wide-spread infectious diseases such as the coronavirus disease 2019 (COVID-19) pandemic continues to storm global health systems significantly, even after five years since its first discovery [1,2]. With the advent of numerous severe acute respiratory syndrome coronavirus 2 (SARS-CoV-2) variants, people worldwide face not only the threat of initial infection but also the prospect of endless reinfections [3,4]. These reinfections may precipitate long-COVID symptoms, fragility, sleep disturbances, cardiac issues, and anosmia that severely impact long-term health and quality of life [5,6].

One of the crucial elements in reducing COVID-19 reinfection is to maintain a substantial concentration of circulating neutralizing antibodies [7–11]. However, the discrepancy in COVID-19 vaccination, the diversity in infected strains, and the varying inoculation time across populations complicate the establishment of a uniform immune background (Figure 1) [12–15]. Effective immunization against COVID-19 pathogens is further complicated by the antigenic drifts of viruses and variations in the immune responses elicited by different vaccines [5,16,17]. This complexity underscores the need for personalized immunization strategies and adaptive public health policies that are responsive to evolving viral landscapes and diverse herd immunity profiles [18]. Interestingly, a definitive quantitative antibody concentration for effective protection has never been established.

The ability to quickly and accurately determine a person's level of protection against COVID-19 is thus crucial for adjusting immunization policies and personal protection plans [8,19–22]. Unfortunately, current techniques for the quantitative evaluation of SARS-CoV-2 binding and neutralizing antibodies fail to become a standard examination in routine disease control operations, due primarily to technical limitations [23,24]. Traditional methods for measuring neutralizing antibodies, such as enzyme-linked immunosorbent assay (ELISA) and live virus neutralization tests (VNTs)/pseudovirus neutralization tests (pVNTs), require large amounts of blood samples and complex laboratory procedures that are not only time-consuming but also susceptible to methodological differences and environmental conditions [25–27]. To overcome these difficulties, recent advanced technologies utilize microvolume samples such as fingertip blood, offering a "perfect match" with microfluidic biosensors [28–31]. However, most of the microfluidic biosensing assays, despite their potential for precision and portability, often grapple with the complex composition of whole blood [32,33], leading to issues such as strong interference with biochemical reagents and low repeatability [34,35]. With only a few exceptions, most of the microfluidic immunoassays do not consider the significance of neutralizing

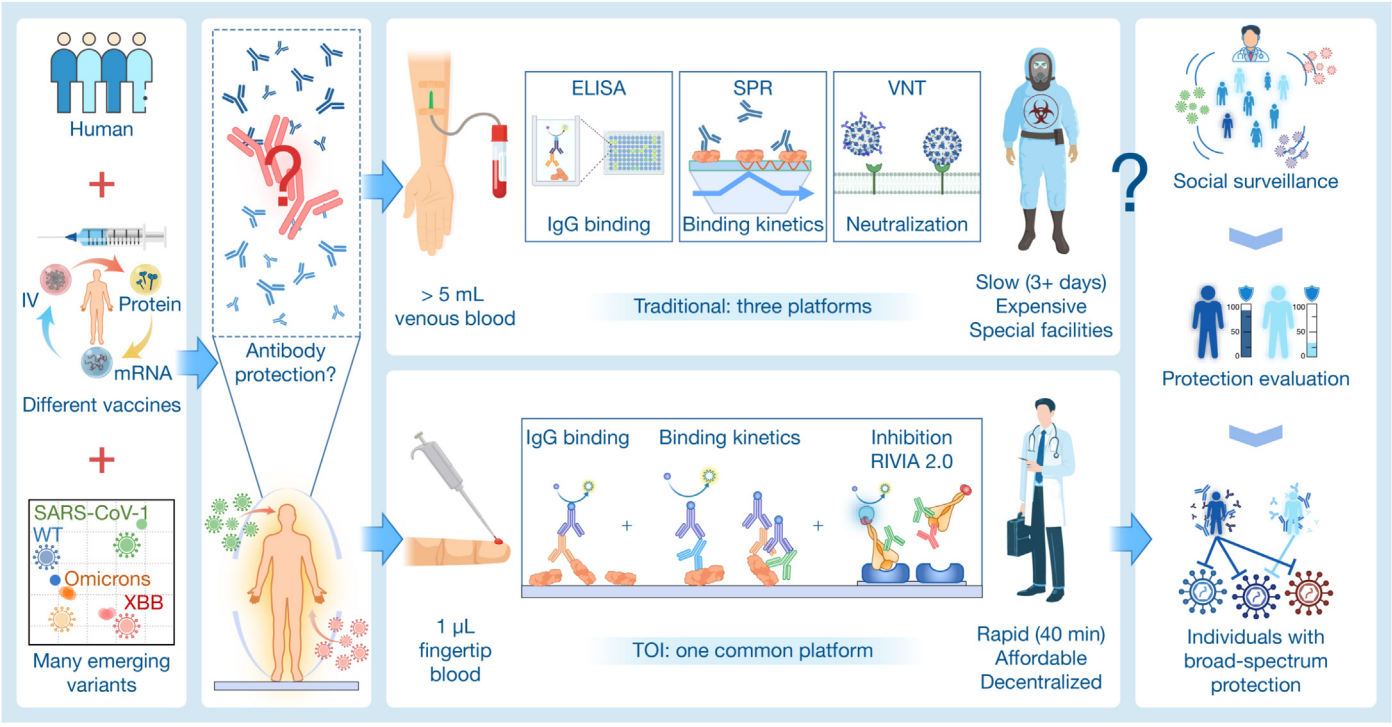

Figure 1. A schematic diagram of the comprehensive humoral immunity protection evaluation for COVID-19 with traditional platforms and the proposed TOI platform

The complicated scenarios stemming from varied vaccination and infection histories affect the evaluation of antibody-related immunoprotection against emerging SARS-CoV-2 variants. Large amounts of blood samples, different test platforms, and types of resources are needed for social surveillance, protection evaluation, and identification of special individuals with the traditional approaches. Abbreviations: COVID-19, coronavirus disease 2019; TOI, tip optofluidic immunoassay; SARS-CoV-2, severe acute respiratory syndrome coronavirus 2; ELISA, enzyme-linked immunosorbent assay; SPR, surface plasmon resonance; VNT, virus neutralization test; IgG, immunoglobulin G; RIVIA, rapid *in vitro* inhibition assay.

antibody evaluation, thus also reducing the utility of their assays [36,37].

In response, we introduce a house-developed tip optofluidic immunoassay (TOI) system (Figure 2). This technology platform leverages the simplicity of fingertip blood collection, enabling rapid and precise immune assessments using microfluidic biosensors. The TOI system is designed to be both user-friendly and efficient, capable of quantifying SARS-CoV-2 binding and neutralizing antibodies within minutes using 1 μL of fingertip blood. For immunoglobulin G (IgG) binding assays, it offers an extremely large dynamic range (4.5 orders of magnitude) and high sensitivity (100 pg/mL). For SARS-CoV-2 neutralizing activity assessments, a renovated version of the rapid *in vitro* inhibition assay (RIVIA) was integrated into the TOI system, allowing for rapid, cost-effective, and robust evaluation with a fraction of the 1 μL fingertip blood sample. Compared with the traditional approaches (Table S1), this economical multifunctional TOI system significantly enhances patient compliance and facilitates decentralized testing, which is vital for effective infectious disease management [38,39].

To validate the reliability and effectiveness of the proposed TOI system, 113 volunteers (135 distinct samples) were recruited for the evaluation of their binding and neutralizing antibody responses against two SARS-CoV-2 strains: wild type (WT) and XBB. Four candidates with significantly high binding and neutralizing antibody levels against a broad spectrum of SARS-CoV-2 strains were identified, demonstrating the graduate shift of the immune spectrum toward the XBB strains circulating in 2023 [40–42]. Moreover, an equivalent concentration of 5 μg/mL SA55 IgG antibody ($TCID_{50}$ [50% tissue culture infectious dose] = ~300–500 in pVNT assays) was estimated to be a cut-off for the high risk of COVID-19 in the coming six months (post measurements). With these technical advancements and comprehensive studies, the TOI system offers a streamlined solution for the screening of individuals with special immune spectrums and the monitoring of herd immunity against new antigenic variants. This multimodal approach is also applicable for population-level immune protection assessment against widespread infectious diseases such as influenza and hepatitis.

RESULTS

TOI-based Fingertip Blood COVID-19 Immunoprotection Evaluation

Evaluating immunoprotection against persistent COVID-19 presents significant challenges due to the complex nature of the pathogen, diverse socioeconomic factors, and technical difficulties [43,44]. The large variation in vaccination status, infections with different viral strains, and highly diverged interpersonal immune responses underscores the need for a comprehensive quantitative assessment of humoral immunity effectiveness.

Such an evaluation requires measuring both the binding antibody levels against the antigen and the neutralization efficacy against the pathogen. Additionally, the binding affinity between patient-derived antibodies and viral antigens can provide valuable insights. However, as shown in Figure 1, the standard approach for comprehensive multimodality evaluation not only

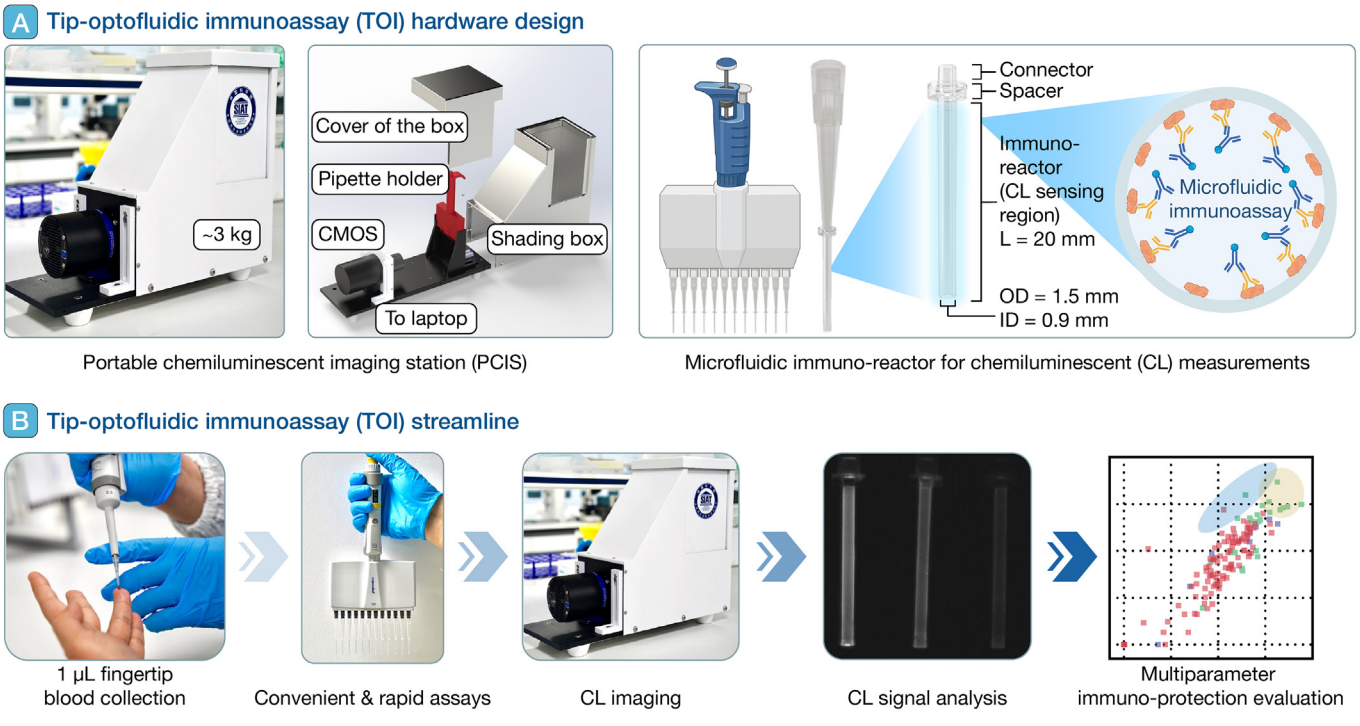

Figure 2. The hardware design and assay streamline of TOI
(A) The hardware used in the design of TOI, including the PCIS for chemiluminescent signal quantification and tip-consolidated microfluidic immunoreactors for CL immunoassays. The microfluidic immunoreactors were operated in batches with multichannel pipettes. (B) The streamline of TOI-based fingertip blood immune protection analysis. Detailed technical information can also be found in Figures S1–S11. Abbreviation: TOI, tip optofluidic immunoassay; PCIS, portable chemiluminescent imaging station; CL, chemiluminescent.

requires a large volume of venous blood (> 5 mL) but also involves three separate, bulky platforms: ELISA for binding IgG quantification, surface plasmon resonance (SPR) for binding kinetics measurement, and VNTs for neutralization efficacy assessment. This comprehensive and multidimensional immunoprotection evaluation is particularly difficult to carry out in resource-limited settings.

To address the challenges in comprehensive COVID-19 antibody protection evaluation, a novel multifunctional TOI system was developed and verified in this study. With 1 μL of fingertip blood, the TOI system was able to complete all three types of assays within 1 h (IgG binding test, binding kinetics, and inhibition efficiency), enabling decentralized surveillance with minimum risk and cost.

The design and hardware parts used in the TOI system can be found in Figure 2A, which relies on polystyrene microfluidic immunoreactors that can be integrated with 200-μL standardized pipette tips (see Supplementary data for detail). The high surface-to-volume ratio of the reactors enables a fast and stable immobilization of concentrated biomaterials followed by efficient chemiluminescent (CL) immunoreactions in the reactors (a detailed theoretical model that describes tubular microfluidic immunoreactors can be found in our recent publication [45]). With a 12-channel pipette, high-throughput testing can be achieved even with manual operation. The signals will be detected using a 3-kg portable CL imaging station (PCIS), which can be used for field studies if necessary. Generally, the multifunctional TOI system and all test procedures established fit the point-of-care needs for immunoprotection evaluation. An illustration of the TOI-based assay streamline can be found in Figure 2B. This house-developed TOI technology was proven to have a pg/mL detection sensitivity and a large dynamic range in sandwich immunoassays for cytokines such as interferon-gamma (IFN-γ) [46].

Establishment and Evaluation of the IgG Binding Assays

With the TOI system developed, we first sought to establish the SARS-CoV-2 spike (S) protein IgG binding assay using three well-calibrated monoclonal human IgGs, SA55, SA58, and D006. SA55 was proved to have broad-spectrum binding and neutralizing activities against almost all strains of SARS-CoV-2 [47,48]. SA58 was also a broad-spectrum antibody against SARS-CoV-2 but lost potent neutralization activity for post-XBB variants. Antibody D006 (Cat#40150-D006) was originally developed against the SARS-CoV-2 receptor-binding domain (RBD) by Sino Biological (Beijing, China). The broad binding spectrum of these antibodies against most SARS-CoV-2 strains has been demonstrated in our previous studies [49].

The experimental design of the demonstration-of-concept study can be found in Figure 3A. The SARS-CoV-2 RBD of

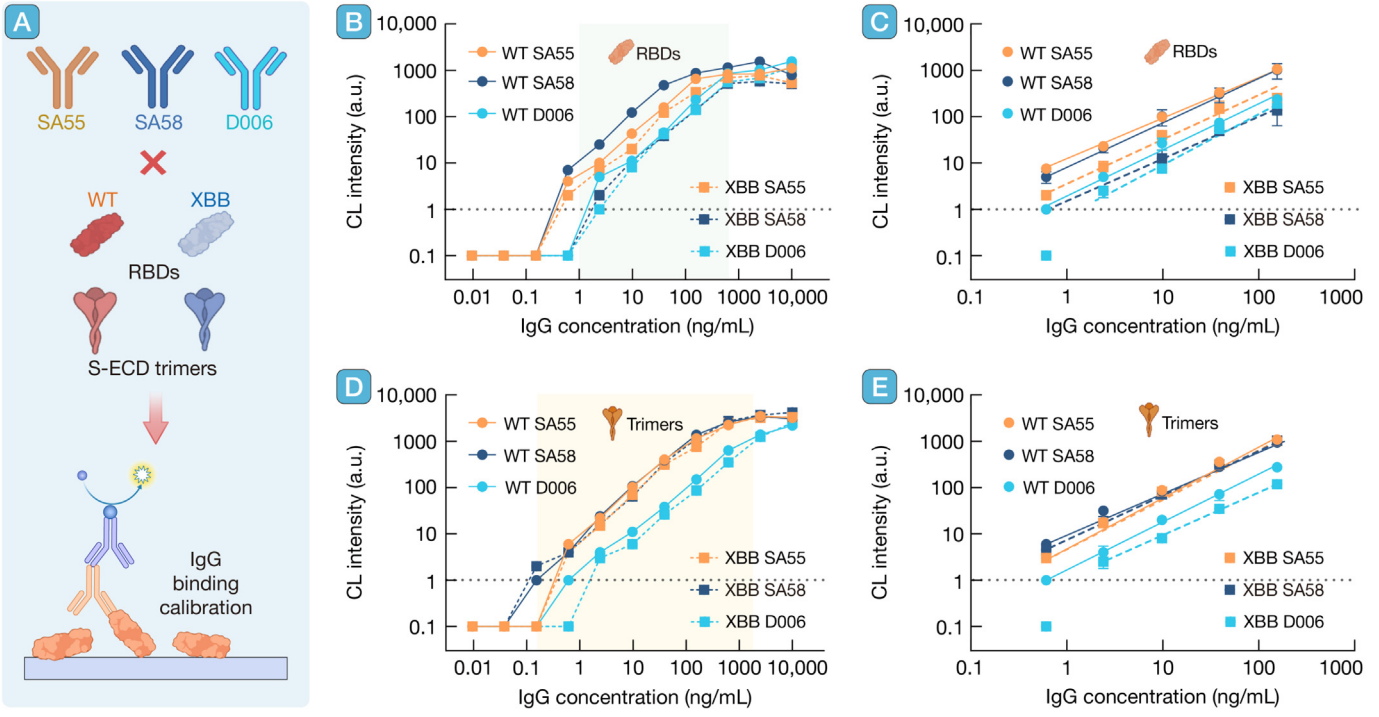

Figure 3. SARS-CoV-2 monoclonal antibody calibration using the TOI system

(A) Conceptual illustration for IgG binding assays. Three monoclonal antibodies (SA55, SA58, and D006) were spiked for evaluation. (B and D) Large dynamic range calibration curves were established with the three monoclonal antibodies that bind to SARS-CoV-2 RBD and S-ECD trimers. The linear dynamic ranges against RBDs and S-ECD trimers are 0.6–600 ng/mL and 0.1–3000 ng/mL, respectively. (C and E) Duplicate calibration curves obtained through linear regressions within the linear dynamic ranges. The error bars generated with RBDs and S-ECD trimers are ~20% and 5%–10%, respectively. The R^2 values for all linear regressions were greater than 0.98 (on log-log scale). Abbreviations: TOI, tip optofluidic immunoassay; SARS-CoV-2, severe acute respiratory syndrome coronavirus 2; RBD, receptor-binding domain; CL, chemiluminescent; a.u., arbitrary units; S-ECD, spike ectodomain; WT, wild type; IgG, immunoglobulin G.

two strains, WT and XBB, was selected as the coating antigen on the microfluidic immunoreactor. The former represents the ancestral strains that should be recognized by the immune system after the injection of inactivated vaccine, and the latter represents the new variants that are not likely under immunoprotection through the vast vaccination in China [50,51]. We also designed and synthesized the trimeric versions of these two S proteins for the IgG binding assays, mimicking the natural form of the protein and a more realistic interaction between the antigen and antibodies.

The calibration curves generated with CL measurements can be found in Figure 3B and 3D with the protocol described in Figure S4A. Note that for all results, the absolute background signals were marked as 0.1, and the minimum quantifiable optical signal for the QHY553M CMOS camera (Beijing, China) is 1.0. As shown in Figure 3B and 3D, the TOI system demonstrates a large dynamic range for IgG binding assays of the three spiked antibodies for both RBD (0.6−600 ng/mL) and spike ectodomain (S-ECD) trimers (0.1−3000 ng/mL). This observation is in accordance with the fact that the homotrimers should have higher structural stability, more binding sites, and thus higher binding affinity than the monomers. The calibration curves constructed for the linear ranges of the IgG binding tests (Figure 3C and 3E) suggest that the TOI system was able to quantify IgGs with 3–4.5 orders of magnitude (in terms of IgG concentration). To note, the calibration curves generated with S-ECD trimers exhibit a much wider dynamic range than those generated with RBDs (details see Figure S12). Even with the 3 orders of magnitude dynamic range for RBDs, the TOI system still outperforms traditional plate-based ELISA in quantification capability as ELISA typically offers only 1.5 orders of magnitude in its dynamic range.

This broad linear dynamic range allows the assessment of antibodies in human blood samples without serial dilution. With the convenient manual operation, the coefficient of variation (CV) of this 12-min IgG binding test ranges between 5% and 20%, which satisfies the requirements for the application. A significant downshift of the XBB RBD binding curves was observed compared with those of the WT strain, but such a phenomenon was not found for the S-ECD trimers. This might be attributed to the increased binding affinity of the trimeric proteins, which compensates for the decrease of antigen–antibody interaction between XBB RBD and spiked IgG.

Evaluation of the Sample Types and Optimization of the IgG Binding Assays

Based on the established IgG binding assays with spiked antibodies, we continued to examine the performance difference of the TOI using four common types of blood samples: fingertip blood, fingertip serum, venous blood, and venous serum (Figure 4A–4B). With the complicated matrix of blood samples from our six volunteers (Z1–Z6), the purposes of these experiments were to verify the robustness of the TOI system across all sample types, as well as determine the optimal dilution factor that provides the highest signal-to-noise ratio.

As expected, the signals of all samples decreased as the dilution factor increased (Figure 4C–4J), with the titration curves of the XBB antigens generally lying below those of their WT counterparts. Similar signal readings were found between the four sample types of the same individual, implying that fingertip blood is likely to be a valid source for antibody studies. The robustness of the TOI system was well illustrated as the IgG titer rankings of the participants remain the same for all antigens. These measurements also identify a large diversity of the IgG levels across the population as the chemiluminescence signals differ over 10 times between Z5 and Z6 at all given dilutions. At the dilution factor of 250, all samples fall into the linear dynamic ranges of TOI (including the strongest and the weakest samples). This argument is valid for the results generated with both RBDs and the S-ECD trimers. As a summary of all previous observations, a single-point dilution at 250× should be enough for quantitative evaluation of the SARS-CoV-2 binding IgG level [52]. In other words, the traditional "titration curve" assays are no longer necessary for TOI-based immunoevaluation. To better quantify the immunoprotection efficacy at the population level while maintaining the distinguishable signals of the background, 250× dilution of fingertip blood will be used. Based on the triplicated measurement results presented in Figure S6, the reproducibility of fingertip blood binding antibody assays at 250× dilutions is remarkably good, indicating that a single-point measurement should be capable of evaluating the IgG binding quantitatively.

We further made a detailed comparison between the signal intensities generated through the 250× diluted fingertip blood samples against RBDs and S-ECD trimers (Figure 4K–4L) as well as the chemiluminescence intensities generated with all four types of diluted samples against the RBDs (Figure 4M–4N). At this dilution level, a strong preference toward the WT RBD is observed, which is generally in accordance with the vaccination and infection history of the participants. Thus, compared to the outcomes of trimers, the results generated with RBD monomers will lead to a better knowledge of antibody binding specificity. Taken together, these experiments suggest that 250× dilutions of fingertip blood can achieve a satisfactory resolution for the immunoprotection evaluation with the TOI system while being convenient and cost-efficient.

Fingertip Blood-based SARS-CoV-2-binding IgG Quantification

With the detection platform being established, the binding antibody for WT and XBB variants was quantified with 1 μL of fingertip blood collected from healthy volunteers. Along with fingertip blood, epidemiological information (vaccination and infection history) and demographical information (age and biological gender) of these volunteers were also recorded.

With TOI and the broad-spectrum antibody SA55 as a calibration standard, absolute quantification of SARS-CoV-2-specific IgG in fingertip blood can be achieved using a single-point dilution of 250× (Figure S13A). This design not only simplified the operation of the experiment but also enabled the evaluation of multiple strains with a limited amount of sample. In addition, we observed that the existence of blood cells in fingertip blood samples does not lead to any significant interference with IgG measurements (Figure S13B).

Due to the difference in vaccine types, inoculation time, infection history, and interperson variations of B-cell response, a

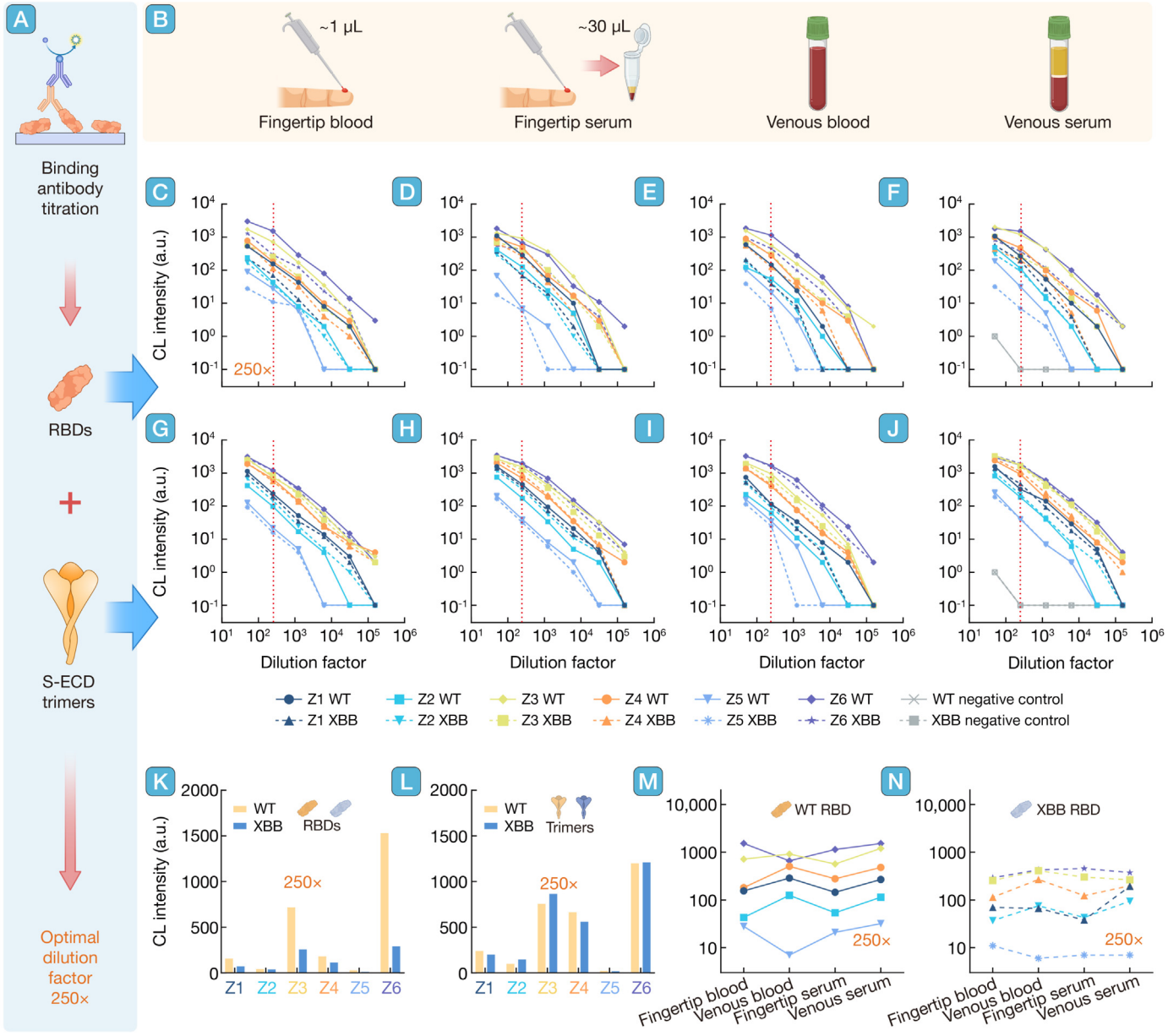

Figure 4. Results of the SARS-CoV-2 IgG binding titration assay, as well as the optimization of parameters

(A) Concept illustration of the IgG binding titration assay, RBDs, and S-ECD trimers from WT and XBB.1.16 strains. (B) Cross-validation of four different sample types: fingertip blood, fingertip serum, venous blood, and venous serum. (C–J) Titration curves were generated with duplicated measurements of 6 participants, Z1–Z6. For all selected antigens, 50-, 250-, 1250-, 6250-, 31,260-, and 156,250-fold dilutions of the four sample types were verified (5× serial dilution). (K–L) Chemiluminescent intensities generated through the 250× diluted fingertip blood samples against RBDs and S-ECD Trimers. (M–N) Similar chemiluminescent intensities were generated with all four types of 250× diluted samples against the RBDs. Abbreviations: SARS-CoV-2, severe acute respiratory syndrome coronavirus 2; RBD, receptor-binding domain; S-ECD, spike ectodomain; CL, chemiluminescent; a.u., arbitrary units; IgG, immunoglobulin G; WT, wild type.

broad concentration range of IgG antibodies (roughly 0.1–1000 ng/mL) was observed across the population (Figure 5A–5B; for raw data, see Tables S2–S3). The binding IgG levels of WT and XBB variants demonstrate strong linear correlations for volunteers with all three types of inoculations (inactivated virus [IV], messenger ribonucleic acid [mRNA], and IV + mRNA/protein), with those who received hybrid vaccination generally showing higher binding antibody levels (Figure 5B, yellow shading). Interestingly, some participants showed better binding affinity toward XBB (Figure 5B, blue shading). We postulate that this phenomenon might be due to the mixed inoculation or recent reinfection.

To further illustrate the variation in binding IgG levels, a series of comparisons were made among the subgroups with different backgrounds (raw scattering plots can be found in Figure S14). As expected, those with mixed inoculation history exhibited significantly higher binding IgG levels for both the WT and XBB RBDs (Figure 5C, $P < 0.0001$ and $P < 0.001$). Since most vaccines were developed with the components of WT viruses, a significantly higher IgG level toward the WT RBD was observed

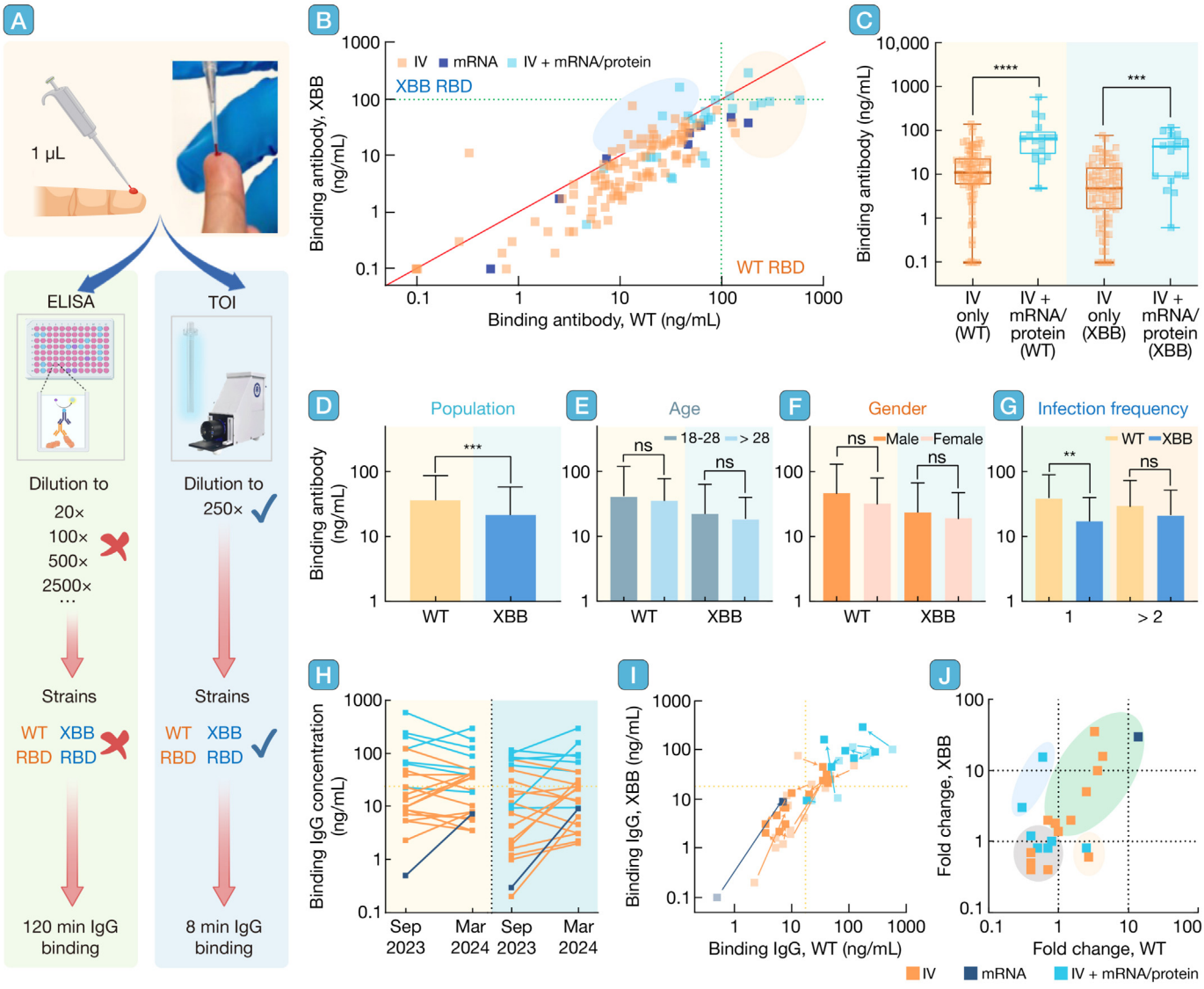

Figure 5. TOI-based large-scale SARS-CoV-2 binding IgG surveillance with single-point dilution of fingertip blood
(A) Comparison of the binding IgG quantification workflow with conventional ELISA and TOI systems. For the TOI-based approach, only less than 1 μL of fingertip blood is needed to quantify the binding IgG level against RBDs of WT and XBB strains, using a single-point (250×) dilution. (B) The scattering plot was generated from 135 samples. Two distinct groups of volunteers with outstanding binding antibody responses were observed (blue and yellow shadings). (C) Box-plot comparison for the effective IgG level against WT and XBB RBDs for volunteers who received different types of vaccines. Higher binding IgG levels were observed for both variants, in the samples collected from volunteers who received more than one type of SARS-CoV-2 vaccine. (D–G) Bar-plot comparisons were generated using different classification approaches (population, age, gender, and infection frequency). All analyses were generated using the same set of data presented in (B). (H) Change of the IgG concentrations for WT and XBB RBD over 6 months for 22 volunteers. (I–J) Scatter plot (I) and the log-scale fold change plot (J) of the longitudinal data, with the color of the spot indicating the inoculation type. The spots in lighter colors represent the test results of samples collected in September 2023, while the darker ones were obtained from resampling in March 2024. The green shading highlights individuals with a proportional increase in WT and XBB IgG, while the yellow and blue shadings identify those who only increase in WT or XBB antibody, respectively. $^{****}P < 0.0001$; $^{***}P < 0.001$; $^{**}P < 0.01$; ns, non-significant. Abbreviations: SARS-CoV-2, severe acute respiratory syndrome coronavirus 2; RBD, receptor-binding domain; WT, wild type; ELISA, enzyme-linked immunosorbent assay; IgG, immunoglobulin G; IV, inactivated virus; mRNA, messenger ribonucleic acid; TOI, tip optofluidic immunoassay.

(Figure 5D, $P < 0.001$). No significant differences between different age groups and genders are found as these factors are independent of infections and inoculation (Figure 5E–5F).

Interestingly, participants who experienced only one prior SARS-CoV-2 infection before sampling appeared to have significantly lower IgG binding antibody levels toward XBB than toward the WT (Figure 5G, $P < 0.01$). For those who were infected more than once, the gap becomes non-significant. In China, the majority of the population got their first infection between late November 2022 and January 2023, with Omicron subvariants (i.e., BA.5 and BF.7) being the predominant strains [53–55]. The second wave was reported to be July–September of 2023, caused possibly by immunoescaped strains in the XBB cluster [56]. Therefore, we postulate that the relatively higher

IgG concentration for the XBB RBD found in the repeated infection population might be due to the second round of immune response for the antigenically drifted variants.

To further verify the application of TOI in convenient surveillance and immune spectrum depiction, a longitudinal study was performed with 22 volunteers, who were sampled and tested twice. Among them, seven demonstrated decreased binding IgG concentrations for both WT and XBB RBDs, 13 showed increased binding IgG concentrations for XBB RBDs, and two showed increased binding IgG concentrations for WT RBDs (Figure 5H and Table S3). The scatter plots for the longitudinal study identified a large variation in the change of IgG antibody levels among the tested population, with the mixed inoculated individuals generally showing the highest absolute IgG concentrations (Figure 5I). Further analysis of the binding IgG fold change during the 6-month period revealed the great differences in immune reaction patterns (for the log-scale, see Figure 5J; for the linear scale, see Figure S15A). As shown in Figure 5J, a group of nine individuals without hybrid vaccination showed a high degree of antibody fold change for both variants (green shading), and two with hybrid vaccination increased only in the fold of XBB-specific IgGs (blue shading). For those with a fold change ≥ 2 for either antibody ($n = 11$), nine appear to have a significant elevation in the IgG level for XBB RBD (81.2%, Figure S15B). Since all 22 participants suffered from flu-like symptoms, only 4 of them confirmed to have SARS-CoV-2 infection during this period (with rapid lateral flow test or transmission chain); all demonstrated significant boosting of XBB IgG concentration (Figure S15B, red triangles). Considering the circulation of XBB-like antigenic strains in China during this period, it is quite likely that recent infections of the XBB variants have led to a second or third round of immune response in these individuals. Upon the series of infections for different antigenic types, their immune spectrums might gradually shift toward the novel antigenic group (XBB). Meanwhile, the original antigenic sin, represented by the IgG antibody levels of the WT vaccine strain, seems to be maintained in the majority of the volunteers. Two individuals only increased in WT IgG levels (yellow shading), although they were very unlikely to be infected by such antigenic type during the period of study.

Comparison of the IgG Binding Kinetics for Volunteers with Different Inoculation Histories

Based on the IgG binding tests of the 135 samples, 18 representatives with high, medium, and low binding affinity were selected for the following binding kinetics analysis. The 250× diluted fingertip blood samples were incubated for 2, 4, and 8 min in the immunoreactors, depicting the change of CL intensities for WT and XBB variants over time (Figure 6A).

As shown in Figure 6B–6C, the CL signals of most participants increased as the incubation time was prolonged, especially between 0 and 4 min. A much higher binding affinity to the WT RBD (∼200–1500 at 4 min) was revealed than that of the XBB (∼100–500 at 4 min). Meanwhile, the seven volunteers with hybrid vaccination (blue) generally demonstrated only slightly stronger binding kinetics (fast increasing of signal and higher levels) than those who received three shots of IV vaccines (orange). A rising trend of the test signals could still be found for the sequential vaccination group when the incubation time increased from 4 to 8 min (blue), implying that the binding of their antibodies to the coated antigens was not saturated yet. The normalized binding kinetics measurement data can be found in Figure S16.

We further compared the migration tracks for IgG binding kinetics collected at 2 min and 4 min with relative signal levels of the assays (Figure 6D). A sharp increase for the majority could be observed at this time interval, indicating the presence of effective binding antibodies and immune protection. Two individuals (one with IV and one with hybrid vaccination) had decreased relative signals for the XBB strain, which might be due to the low signal levels for this variant or the resolution reduction at a high dilution factor (250×).

To better illustrate the difference in IgG binding kinetics for participants, the test results were reanalyzed based on the different vaccination histories (Figure 6E). Less interpersonal variation was observed for the WT, possibly because the IV vaccine received by all participants (at least once) was generated based on this antigenic group [57,58]. For the XBB antigenic group, however, the large diversity might be caused by different infection histories (i.e., recent XBB variant infection) or immune responses. With a limited amount of data, only a slight difference is observed between the two groups for the WT strain. No significant binding affinity difference can be found for the IgG against the XBB RBD. Such results imply that different types of vaccination do not lead to qualitative differences in antibody potency/affinity.

RIVIA 2.0 Based on the TOI Platform

Inspired by the conventional inhibition tests and our previous analytical system [59,60], in Figure 7A, an upgraded version of the RIVIA 2.0 was developed based on previously developed RIVIA 1.0. In the current experiment, specially engineered human ACE2 (hACE2)-human Fc (hFc) and Avi-tag biotinylated S-ECD homotrimers were designed and constructed, with the former coated on the stationary phase of the immunoreactors (see Figures S8–S9). The S-ECD monomers trimerized automatically through the trimerization domain and would bind to the hACE2 receptor with high affinity and maximal signal level in the absence of antibody inhibition (Figure 7A–7B).

To establish RIVIA 2.0, the inhibition efficiency curves of three standard antibodies, SA55, SA58, and D006, were constructed for WT and XBB S-ECD homotrimers (Figure 7C–7D). As shown in Figure 7C, the inhibition curves of SA55 and SA58 were similar for the WT protein (dynamic range of the spiked antibodies: 10−1000 ng/mL), while that of the D006 was almost flat. The inhibition profiles of SA55 and D006 antibodies remained consistent for the XBB protein, whereas a marked decrease in inhibition efficiency was observed for SA58, likely due to emerging immune escape mutations compromising its effectiveness [61,62]. These findings were partially consistent with the results of IgG binding assays (Figure 3D–3E), where the binding affinity of D006 to the trimeric antigen was much lower [52]. However, due to the difference in reaction mechanisms (Figures 3A and 7A), the distinct interacting patterns of SA55 and SA58 could only be

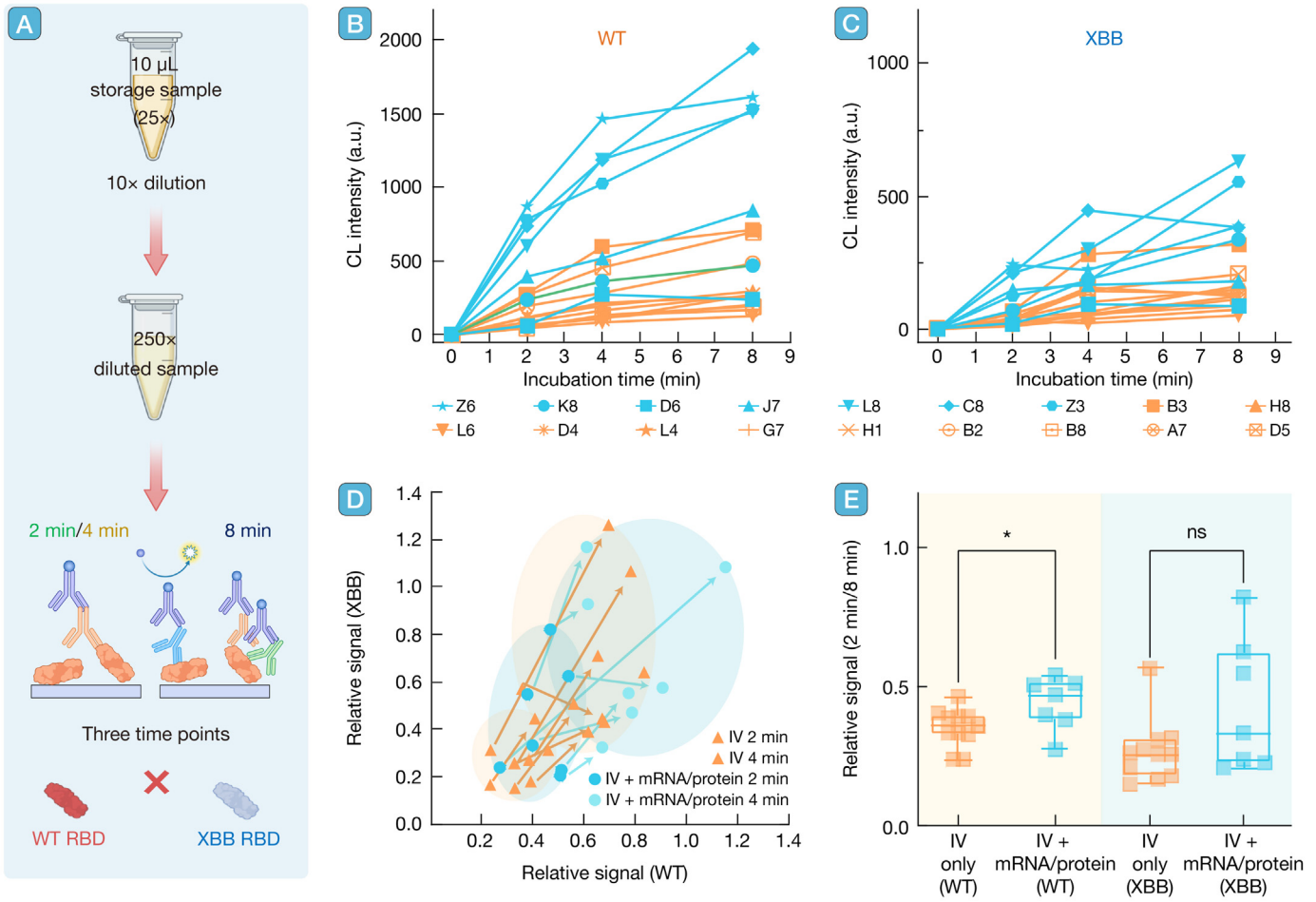

Figure 6. Results and analysis for the SARS-CoV-2 RBD-specific IgG binding kinetic studies with TOI
(A) An illustration for the sample preparation and assay procedure. The 250× diluted fingertip blood samples from 18 representative volunteers were incubated for 2, 4, and 8 min. The RBDs of SARS-CoV-2 WT and XBB strains were used as the target antigen. (B–C) The IgG binding kinetic curves against WT and XBB RBDs. The orange dots and lines indicate the 11 volunteers who received the COVID-19 inactivated virus (IV) vaccine, while the blue ones indicate the rest seven individuals who received more than one type of vaccine. (D) The migration track of the relative signals for IgG binding kinetics collected at 2 min and 4 min. (E) Comparison of the IgG binding affinity against WT and XBB RBDs for volunteers with different inoculation histories (incubation time = 4 min). Borderline significance was observed for the WT RBD, but no significant difference was observed for the binding affinity against XBB RBD. *$P < 0.05$; ns, non-significant. Abbreviations: COVID-19, coronavirus disease 2019; SARS-CoV-2, severe acute respiratory syndrome coronavirus 2; WT, wild type; RBD, receptor-binding domain; CL, chemiluminescent; a.u., arbitrary units; TOI, tip optofluidic immunoassay; IgG, immunoglobulin G.

observed in the inhibition tests (Figure 7D). We further evaluated the repeatability of RIVIA 2.0 with 1 μg/mL SA55- and SA58-spiked samples and found that the system is quite stable (CV: 0.8%–1.9%) at high inhibition efficiency (~95%). As the inhibition efficiency decreases to ~50%, the CV rises to 22.6%, which is still within the acceptable range for manual operation using a fingertip blood-based convenient system.

Since this is the first comprehensive evaluation of the TOI platform and RIVIA 2.0, cross-validation was performed between TOI-based RIVIA 2.0 assays and the standard SARS-CoV-2 pVNTs (Figure 7F). A total of 31 volunteers participated in this second round of the study. Using the inhibition efficiency obtained from RIVIA 2.0 (50× dilution of fingertip blood) as the vertical axis and the calculated dilution factor of the pVNT using venous serum samples as the horizontal axis, a strong correlation was observed for the WT strain, indicating good agreement between the two systems. However, a weaker correlation was noted for the XBB variant, likely due to the lower overall inhibition efficiency reported by RIVIA 2.0 at the fixed 50× dilution. As suggested by the precision tests (Figure 7E), higher inhibition efficiency (> 30%) generally improved the confidence level of RIVIA 2.0. Therefore, for the real-world inhibition evaluation against SARS-CoV-2 later variants (e.g., XBB or other strains that appeared after 2024), a lower dilution factor for RIVIA 2.0 (e.g., 10× or 5×) is more appropriate.

Following the successful cross-validation, a further comparison was made between RIVIA 2.0-based inhibition efficiency and the effective binding IgG levels of the volunteers (Figure 7G). Strong correlations were observed for both strains, with slightly higher effective binding IgG levels and inhibition efficiencies observed against the S proteins of the WT strain.

Despite the large interpersonal variability and limited sample size, four out of the 31 participants demonstrated potent and broad-spectrum inhibition protection against both the WT and

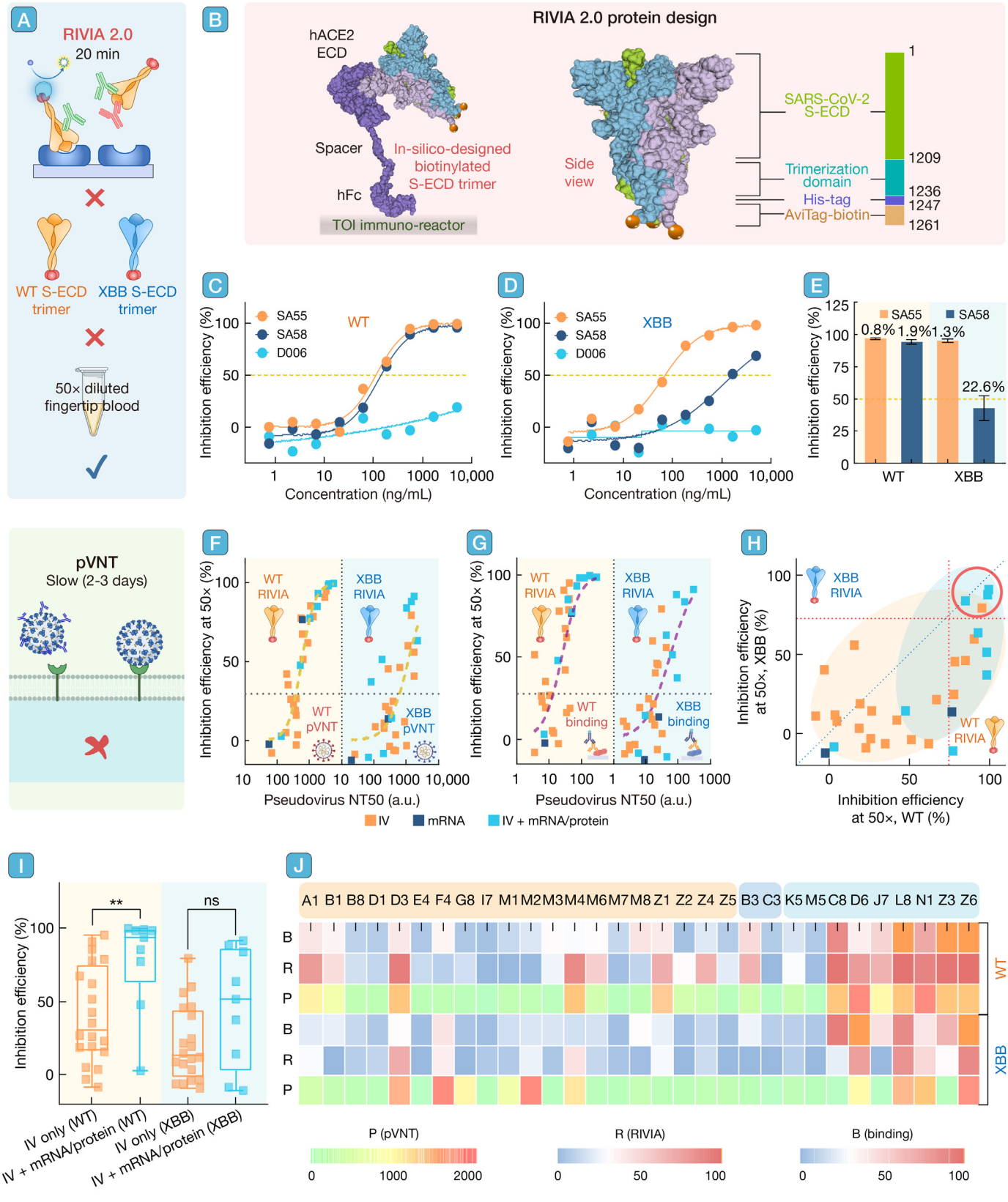

Figure 7. The development, evaluation, and application of the TOI-based renovated rapid *in vitro* inhibition assay (RIVIA 2.0) using a single-point dilution strategy

(A) Conceptual illustration and comparison of the RIVIA 2.0 evaluation procedure, in comparison with conventional pVNT, followed by the fingertip blood samples. (B) Structural illustration of the engineered hACE2-hFc and Avi-tag biotinylated S-ECD homotrimers used in RIVIA 2.0. (C–D) Broad-range calibration curves established with the three monoclonal antibodies against Avi-tag biotinylated S-ECD trimers from WT and XBB strains. (E) The CVs of RIVIA 2.0 obtained with 6 repeated tests of 1 μg/mL SA55 and SA58 as mock samples. (F–J) Applications of the RIVIA

(legend continued on next page)

XBB strains (Figure 7H, red circle). Participants who received mixed inoculations were more likely to exhibit higher binding IgG levels and inhibition efficiencies (Figures 5C and 7I). A heatmap summarizing all test results, including binding IgG levels (B), RIVIA inhibition efficiency (R), and pVNT neutralization results (P) for both the WT and XBB strains, is presented in Figure 7J, further supporting the consistency between different methods and assays.

Since none of the participants had been naturally infected with the WT strain, the observed protection was likely induced by a hybrid immunization process, involving pre-infection vaccination (with vaccines primarily developed against the WT strain) followed by 1–2 natural infections dominated by BA.5, BF.7, and XBB.1.5 strains. Notably, the hybrid vaccination strategy (IV + mRNA) provided more potent and broad-spectrum antibody protection than did immunization with IV alone. These individuals probably exhibit distinct cellular-level immune responses due to their hybrid inoculation strategy, which uniquely stimulates the immune system. However, it remains unclear whether the broad-spectrum protection observed is attributable to a single set of broadly neutralizing B-lymphocytes or a combination of different B-lymphocyte clones, each targeting specific strains. In-depth single-B-cell analysis will be conducted in our follow-up studies.

To further enhance the protective efficacy of SARS-CoV-2 vaccines, particularly against future variants, another strain with a greater antigenic distance from both the early WT and XBB variants, such as JN.1 or KP.3 (Figure S19), could be a promising candidate. Moving forward, a longitudinal diagnostic study will be conducted to monitor antibody level changes in a cohort following multiple SARS-CoV-2 infections with different strains. Additionally, a side-by-side comparison between TOI-based antibody protection assessment assays and single-cell B-cell immune response analyses should be performed. In such studies, the TOI platform could continue to serve as a valuable resource for immune-response monitoring while offering critical insights into community immunization strategies.

DISCUSSION

Technical Discussion and Directions for Improvements

During the collection process of volunteer samples, fingertip serum was found to be an unfavorable sample type. Due to the relatively large volume requirement (~30 μL), we experienced challenges in collecting enough fingertip serum from volunteers. Comparatively, 1 μL of fingertip whole blood was much easier to collect and enough for conducting both the RBD-binding IgG quantification and inhibition activity quantification with the TOI (Figure S17). The results generated with fingertip blood closely mirror those obtained from traditional venous serum and whole blood samples, validating the reliability of fingertip blood as an equivalent source for antibody testing. Undoubtedly, fingertip blood-based assays are more practical and less invasive, particularly beneficial for the herd immunity surveillance of COVID-19.

In addition, our findings suggest that RBDs may offer a slight advantage in IgG binding specificity evaluation, compared with full-length S-ECD homotrimers (Figure 4K). Such an advantage is highly likely provided by the smaller protein size (more sensitive toward single-point mutations). However, a narrow dynamic range was observed for assays using RBDs compared to those using S-ECD homotrimers (caused by physical limitations of the available binding space). With the optimized 250× dilution of the fingertip blood, the RBD-based IgG binding assays can effectively and quantitatively distinguish samples with higher or lower antibody abundance within the linear dynamic range. This optimization is crucial for accurate and effective assessment of antibody-based immunoprotection at individual and population levels.

For the volunteer-based SARS-CoV-2 RBD-binding IgG level assessment study, we observed a wide distribution of the effective antibody concentration among healthy volunteers with various immunization backgrounds. Multiple volunteers showed < 0.1 ng/mL and > 100 ng/mL of effective SA55 concentration for both WT and XBB strains, indicating a strong interperson diversity of the COVID-19-specific antibody immune response. Given the large dynamic range (3–4 orders of magnitude) of TOI, absolute IgG quantification with a single-point dilution can be achieved. This is particularly advantageous compared to conventional ELISA, which generally requires multiple-point titration curves due to its relatively small dynamic range (1.5 orders of magnitude), making it incompatible with small-volume samples such as 1 μL of fingertip blood.

Based on the infection history and epidemiological information provided by the volunteers, we found that vaccination contributed the most toward the binding antibody level: those with more than one type of inoculation (typically IV + mRNA or IV + recombinant protein [RP]) tend to have higher effective antibody concentration for both strains. In addition, volunteers who suffered from reinfection tend to have a stronger antibody immune response toward the XBB strain, leading to an improved antibody binding spectrum. Based on the COVID-19 epidemiology records in China in 2023, it is highly possible that the second wave (summer–fall in 2023) of infection was caused by a variant in the XBB cluster [63].

2.0 performed with blood samples of 31 representative volunteers. (F) Cross-validation between RIVIA 2.0 using single-point dilution and the standard SARS-CoV-2 pVNT based on multiple dilution points. (G) Cross-validation between RIVIA 2.0 and the binding IgG level for WT and XBB strains. (H) Side-by-side analysis of fingertip blood samples for the binding inhibition efficiencies against the WT and XBB strains. Four candidates with strong and broad-spectrum inhibition efficiencies were identified and were labeled as the points in the red circle. (I) Comparison of volunteers with different inoculation histories for their IgG binding inhibition efficiencies against WT and XBB strains. (J) Summarization of the binding IgG level (B), RIVIA 2.0 inhibition efficiency (R), and pVNT neutralization activity (P) of volunteers (raw data see Table S4). The four individuals with outstanding inhibition efficiencies (red circle in Figure 7H) were Z6, L8, D6, and D3. All results generated with TOI (binding IgG level and RIVIA 2.0 inhibition efficiency) were visualized with the blue-red color bar, while the pVNT neutralization results (P) were presented with the green-red color bar. $^{**}P < 0.01$; ns, non-significant. Abbreviations: CV, coefficient of variation; hACE2, human ACE2; hFc, human Fc; IgG, immunoglobulin G; pVNT, pseudovirus neutralization test; SARS-CoV-2, severe acute respiratory syndrome coronavirus 2; S-ECD, spike ectodomain; TOI, tip optofluidic immunoassay; WT, wild type.

Based upon our fingertip blood-based longitudinal investigation of humoral immunity, we estimated a cut-off IgG concentration which can be potentially applied in short-term (6 months) infection risk predictions. As presented in Figure S18, when using 20 ng/mL of WT RBD-binding IgG as the cut-off level (5 μL in the original serum, before dilution), the chances of SARS-CoV-2 infection were 81.8% and 27.3% for the two groups. When using 20 ng/mL of XBB RBD-binding IgG as the cut-off level, the chances of SARS-CoV-2 infection were 76.9% and 33.3% for the two groups. Such concentrations can also be correlated with $TCID_{50}$ = 300−500, which is a reasonable level for establishing an effective COVID-19 immunoprotection (Figure S19). Interestingly, we observed a balancing effect around 20 ng/mL of binding IgG. People with higher antibody levels tend to decay to somewhere around this concentration. People with lower antibody levels tend to get COVID-19, thus bringing the IgG level back to around 20 ng/mL. Although the threshold was preliminary and derived from a limited dataset, our findings suggest that the abundance of RBD-binding IgG (targeting the most up-to-date variant) may serve as a promising biomarker for predicting near-term infection risk (up to 6 months post measurement). With a different sample collection/storage methodology (based on venous blood) and a larger tested population, a similar phenomenon has been reported by Kenny et al., suggesting that the RBD IgG thresholds could also help to predict protective host immunity for SARS-CoV-2 and help guide vaccination strategies [64].

Our observations also indicate a gradual override of ancestral WT immune imprinting in individuals infected with the Omicron variant, followed by XBB strains in mid to late 2023 [54,56], supporting the hypothesis that sequential exposure to antigenically distinct variants may mitigate the antigenic sin [65]. Among 22 resampled individuals, we identified two individuals with boosted WT antibody levels, likely due to strong immune imprints [66,67]. Thus, the TOI system is particularly suited for depicting heterogeneous immune profiles and identifying individuals with unique immune responses, which could aid in studies of unusual immune mechanisms, such as extremely weak antibody responses or post-acute sequelae.

Despite the significant variation in effective concentrations of SARS-CoV-2 RBD-binding IgG across the volunteer population, antibody binding kinetics appeared to be similar for most individuals. Only slightly improved IgG binding affinity was observed in volunteers who received multiple types of vaccines compared to those with three shots of IV vaccine. This observation can be explained as the affinities of SARS-CoV-2 RBD-binding IgG may be intrinsically limited by the antibody maturation mechanism in the lymphatic system. Our findings indicate that IgG binding affinity measurements may be unnecessary for routine surveillance and infection risk prediction.

After years of discussion, it has become a consensus that the neutralization/inhibition activity in circulating blood is also a crucial factor in the evaluation of SARS-CoV-2 immunoprotection level. However, traditional cell-based VNTs and pVNTs suffer from long assay times, high facility requirements, and high material and labor costs, thus limiting the virus neutralization assays from the routine practice of disease surveillance. In our previous work, a prototype RIVIA was developed to mimic the neutralization/inhibition process in microfluidic immunoreactors. However, the S-ECD protein used as the "mock virus" in RIVIA 1.0 lacked a signaling domain, making the chemical biotinylation step indispensable. Such a modification with low reaction site-specificity was prone to undesirable binding interference and increasing risk of non-specific background noise.

In the current study, the S-ECD trimer proteins were re-engineered by adding an integrated Avi-biotin tag at the N-terminal, achieving site-specific/orientation-specific biotinylation. With the renovated protein probes (hACE2-hFc and Avi-tag-biotinylated S-ECD homotrimers), the working concentration of the S-ECD protein probe was reduced significantly from 140 ng/mL to 10 ng/mL in the RIVIA 2.0 system. Meanwhile, the total assay time was shortened to 20 min, which was significantly faster than all types of VNTs/pVNTs (roughly 2−3 days), as well as RIVIA 1.0 (90 min). Furthermore, the incorporation of an Avi-biotin tag at the terminus of the S-ECD homotrimer significantly enhances signal uniformity in TOI and improves test reproducibility. This improvement may be attributed to the Avi-biotin tag's ability to stabilize the spatial orientation of the S-ECD homotrimer.

Note that the dynamic range for RIVIA 2.0 is also tunable by changing the sample incubation time (Figure S20). For measurements with fingertip blood samples, a good correlation between the RIVIA 2.0 and conventional pVNT was observed (Figure 7). We also noticed that the measurements with fingertip blood samples and venous serum samples were slightly different but generally shared the same trend (Figure S21).

Despite the advantages of the TOI system and RIVIA 2.0, continuous technical improvements are still necessary. When the inhibition efficiency measurement results are lower than 30%, the CV is considerably large (∼20%), leading to high uncertainty in quantitative measurements. In addition, the dynamic range for RIVIA 2.0 covers only approximately 2 orders of magnitude due to the saturation of signals. More advanced synthetic biology approaches are needed to enhance the dynamic range at both ends. Alternatively, two different dilution factors (i.e., 20× and 200×) may be used instead of the single-point dilution measurements in this study to improve the dynamic range for individuals with different antibody protection levels.

In summary, a TOI system was developed for comprehensive antibody protection evaluation against multiple SARS-CoV-2 strains using 1 μL of fingertip blood. Benefitting from the high performance of the microfluidic immunoreactors and the CL imaging station, TOI can achieve a lower limit of detection (LLOD) of 0.1 ng/mL (for IgG binding) and a dynamic range of 3−4.5 orders of magnitude, with an exceptionally high signal-to-noise ratio (∼10,000). Meanwhile, inhibition activities against multiple variants can be measured within only 20 min, providing a much faster platform for neutralization efficiency screening, and setting a new benchmark for convenient COVID-19 antibody assays.

Compared to existing microfluidic and lateral-flow assay-based detection technologies that can only provide qualitative or quantitative results of antibody binding, our method enables the simultaneous assessment of both antibody binding and neutralizing capabilities through minimal (1 μL) fingertip blood sample consumption. Integrating our findings in RBD-binging

IgG measurements and inhibition efficiency measurements, we have identified four volunteers with outstanding antibody protection spectrum and protection levels against multiple SARS-CoV-2 strains. Our technology platform will lead to higher potential in finding broad-spectrum and high-affinity neutralizing antibodies against not only SARS-CoV-2 but also other viruses in the sarbecovirus family. In the future, such antibodies discovered by our outstanding volunteers may be able to serve as the first line of defense in the war against the "next" coronavirus pandemic.

Future Perspectives

Taking advantage of the convenient multifunctional TOI system, binding IgG quantification and inhibition efficiency measurements can be incorporated into a single platform using just 1 μL of fingertip whole blood. As the emergence of SARS-CoV-2 antigenic variants is inevitable (e.g., the JN.1 strain cluster in 2023–2024, see Figure S22), new solutions for rapid, safe, affordable, and decentralized surveillance remain critical [68,69]. In this permanently ongoing study, we are also exploring revolutionary approaches for the collection, transportation, and storage of fingertip blood samples.

One of our significant findings is the identification of a cut-off RBD-binding IgG concentration for short-term infection risk prediction. However, the current sample size is insufficient for definitive conclusions on infection–risk prediction accuracy. With support from relevant authorities, we aim to expand this risk prediction study to over 10,000 volunteers for more comprehensive decentralized surveillance.

In the long term, we plan to develop a fingertip blood-based immunoprotection model that includes both antibody protection data and pathogen-specific T-cell and B-cell responses. Preliminary results from our ongoing study using a coherent microscale interferon-gamma release assay (CM-IGRA) for T-cell response analysis show promising outcomes for various infectious diseases [46]. Due to the nature of low sample consumption, TOI will still play a main character in the data collection procedure in the model establishment process.

Compared to existing microfluidic and lateral-flow assay technologies that provide only qualitative or quantitative antibody binding measurements, our method enables the simultaneous assessment of both antibody binding and neutralizing capabilities using a minimal 1-μL fingertip blood sample. By integrating our findings from RBD-binding IgG measurements with inhibition efficiency assessments, we have identified four volunteers exhibiting exceptional antibody protection—both in spectrum and level—against multiple SARS-CoV-2 strains. In the future, TOI-based immune protection assessment could be extended to applications in public health and disease control. For example, it may be used to distinguish antibody responses induced by smallpox vaccination *versus* those generated by natural mpox infection. The design of such studies may benefit from the integration of artificial intelligence (AI) to aid in antigen design [70].

Beyond epidemiologic studies and disease control applications, the TOI system holds potential for vaccine and therapeutic antibody development. The throughput of TOI can be boosted with only minor technical modifications, facilitating a rapid screening and quantitative evaluation of therapeutic or immunization efficacies. With minimal risk and blood consumption, continuous monitoring of the dynamic IgG pattern for the same individual or experiment animal becomes much easier [71].

In conclusion, the highly compatible and convenient TOI system is poised to empower cutting-edge research and timely disease control efforts from multiple perspectives in future pandemics. By integrating rapid, precise antibody assessments with minimal sample requirements, the TOI system enhances our ability to respond to emerging infectious threats and supports the development of personalized protection and immunization strategies.

MATERIALS AND METHODS

Portable Tip Optofluidic Immunoassay System

The TOI system is composed mainly of two sections: first, microfluidic immunoreactors and second, PCIS. The immunoreactors are used as disposable structures for conducting immunosorbent assays with fingertip blood samples; the CL imaging station is designed to quantitatively measure the CL signal intensities of the immunoreactors (Figure 1). Detailed information for the two sections can be found in the following paragraphs.

Microfluidic Immunoreactors

The microfluidic immunoreactors were fabricated through injection molding with high-protein affinity polystyrene, with technical support from Beijing 4.0 Industrial Technology Co., Ltd (fabricated in Shenzhen, Guangdong, China). The microfluidic immunoreactors are composed of three units: a sensing unit, an intersection, and an adapting unit. The inner diameter of the microfluidic immunoreactors is 0.9 mm. As presented in Figure S1A–S1D, the industrial-grade mass microfabrication of the reactors could achieve a qualified yield of over 99.9% for each batch of product (∼10,000), indicating a high reliability. To perform an immunoassay, the microfluidic immunoreactors will be connected to standard 20- to 200-μL pipette tips for liquid handling. No chemical surface treatment is needed before each immunoassay. The evaluation of protein immobilization kinetics for the microfluidic immunoreactors is shown in Figure S2A. For common proteins such as IgG, physical adsorption generally saturates after 20–40 min, which is significantly faster than conventional immunoassay reactors like 96-well plates. In our other research applications, this house-developed TOI technology was proved to have a 3-pg/mL detection sensitivity and 4 orders of magnitude dynamic range in sandwich immunoassays for cytokines such as IFN-γ.

Portable Chemiluminescent Imaging Station

To simplify the platform structure to the greatest extent, the chemiluminescence imaging method was chosen for immunoassay signal measurement. The PCIS was designed and assembled in-house. As presented in Figure S3, the PCIS includes a shading cover (stainless steel), a pipette holder (also works as the immunoreactors), and a CMOS camera. The total weight of the signal measurement box is about 3 kg, which is easy to carry with one hand.

The intensity of the chemiluminescence signal is generally very weak. Thus, the protection against environmental light interference is a key factor in the design of the signal measurement

box. Light-protection structures are placed in all corners and connecting sections. To perform accurate and quantitative measurements of the CL system, we used a highly sensitive monochromic CMOS camera QHY533M (from QHYCCD, Beijing, China) along with a Fujinon wide-angle microdistance lens to collect long-exposure CL images. The camera is placed 12.5 cm in front of the pipette holder. The pipette holder (fabricated through three-dimensional printing) is designed to stabilize the multi-channel pipette and the attached immunoreactors attached. Vertical walls are built between the microfluidic immunoreactors to prevent inter-channel crosstalk.

The optical quantification performance of the QHY533M camera can be found in Figure S2B. The minimum detectable optical signal intensity was 1.0, and the linear dynamic range was about 60,000 (at gain = 70), covering 4.5–5 orders of magnitude in optical signal intensity.

Chemiluminescent Signal Quantification

After the final reaction step, the multi-channel pipette with the microfluidic immunorectors will be placed in the PCIS for chemiluminescence intensity measurement. The baseline is calculated as the average blank signal intensity for the device. Based on our optimization results, a 6-s exposure time is suitable for most of the chemiluminescence intensity quantification applications.

Biomolecular and Chemical Reagents

All fundamental chemical reagents, including 10× phosphate buffered saline (PBS) buffer, pH = 7.4 (Thermo Fisher, Massachusetts, USA; Cat#AM9624), wash buffer (0.05% Tween-20 in PBS), and luminol chemiluminescence substrate (SuperSignal™ ELISA Femto Substrate; Thermo Fisher, Massachusetts, USA; Cat#37075) were purchased from Thermo Fisher (Massachusetts, USA). All protein buffers, including 10% Blocker™ BSA (in PBS, Thermo Fisher, Massachusetts, USA; Cat#37525), 1% casein (in PBS, the product name was called the poly-horseradish peroxidase [poly-HRP] dilution buffer, Cat#N500), and SuperBlock™ buffer (in PBS; Thermo Fisher, Massachusetts, USA; Cat#37515) were also purchased from Thermo Fisher.

For biomolecular reagents, broad-spectrum SARS-CoV-2 antibodies SA55 and SA58 were developed and provided by Dr. Yunlong Cao from Peking University. Recombinant SARS-CoV-2 RBDs (40592-V08H for WT, 40592-V08H136 for XBB.1.16), recombinant SARS-CoV-2 S-ECD homotrimers (40589-V08H8 for WT, 40589-V08H48 for XBB.1.16) and recombinant SARS-CoV-2 antibody D006 (Cat#40589-D006) were all produced and provided by Sino Biological (Beijing, China). The monoclonal anti-human-IgG antibody (HRP conjugated) was also developed and provided by Sino Biological (Cat#68090-MM04-H). The streptavidin-labeled poly-HRP (SA poly-HRP) was purchased from Thermo Fisher (Massachusetts, USA; Cat#21140).

Assay Protocol with Recombinant SARS-CoV-2-specific Human IgG

For SARS-CoV-2 IgG binding assays with recombinant antibodies, antigenic proteins (RBDs or S-ECD homotrimers) were first immobilized on the inner surface of the immunoreactors. The working solution of protein was in 1× PBS (pH = 7.4) at 10 μg/mL. Two consecutive blocking steps (3% BSA in PBS + SuperBlock™ buffer) were used to reduce the noise level. The immunoreactors were rinsed once after each incubation step. A graphical illustration of the assay protocol can be found in Figure S4.

For concept demonstration, standard antibody solutions at different concentrations were tested with TOI. Three recombinant SARS-CoV-2 IgGs (SA55, SA58 [56,72], D006 [52]) were evaluated in this assay (Figure 2). The working solutions of the antibodies were first prepared by diluting the stock solution with 1% casein in PBS. Four-fold serial-diluted antibody solutions were drawn into the reactors to react with protein immobilized on the reactor's inner surface and left at room temperature to react. The incubation time for the antibody solutions was 8 min. Subsequently, an HRP-conjugated detection antibody solution (6000× diluted with 1% casein in PBS, ~170 ng/mL) was applied to the immunoreactors. The incubation time for the detection antibody solutions was 3 min. Finally, a CL substrate was introduced to the immunoreactors after rinsing in triplicate. The optimization of the blocking and dilution buffer can be found in Figures S5–S6. Using 1% casein in PBS for both immunoreactor blocking and sample/reagent dilution significantly reduced the background noise level to a nearly non-detectable level.

Human Sample Collection

With the informed consent of all participants, venous blood samples were collected by trained experts using vacuum blood collection tubes, while fingertip blood samples were collected with pain-free fingertip blood pens that were designed for routine blood glucose monitoring. Fingertip serum samples were generated by centrifuging 30 μL of fingertip blood for 3 min at 3000 g. For all volunteers, the fingertip blood was diluted 25× using 1% casein in PBS, followed by a quick spin for the removal of the pellet (i.e., red blood cells) before storage at –20 °C (Figure S7). All other types of samples were also diluted with 1% casein in PBS before applying to TOI. The first round of sample collection was conducted in September 2023, involving 113 individuals. The second round of sample collection was conducted in March 2024, involving 22 individuals from the first round of sample collection. The negative-control sample was obtained from one of our previous clinical studies, which was approved by the IRB of the Second Affiliated Hospital of Chongqing Medical University (No. 2018 (100)) [73]. The blood sample was collected in 2019 (before the COVID-19 outbreak) and stored at –20 °C without freeze and thaw ever since. The informed consent of this study was obtained through recontact of the healthy blood donor of the sample.

Binding IgG Titration Curves for Different Sample Types

The binding IgG titration assays for different sample types were conducted with blood samples of six volunteers using a protocol that was generally consistent with the proof-of-concept experiments. To generate a six-point titration curve for SARS-CoV-2-specific IgG, whole blood/serum was prepared and stored, as described in the previous section. Various final concentrations

were prepared by further diluting the stock solution with 1% casein. The final dilution factors of the samples were 50, 250, 1250, 6250, 31,250, and 156,250 folds. A negative-control serum collected before the COVID-19 outbreak (without SARS or Middle East respiratory syndrome [MERS] infection history) was also applied and served as a baseline for the TOI (Figure 3).

Binding IgG Quantification and Binding Kinetic Evaluation of the Blood Samples

In the SARS-CoV-2 binding IgG quantification study, 1 μL of fingertip blood was evaluated for 135 volunteer samples (Figure 4). All volunteers were numbered for deidentification during testing. However, their background information including age, gender, COVID-19 vaccination records, and infection history were recorded upon participation and unblinded upon data analysis. To evaluate the SARS-CoV-2-specific IgG binding capacity of volunteers quantitatively, the results of this assay were converted to the equivalent concentrations of a therapeutic antibody, SA55 [72]. The effective SA55 concentration was measured with a three-point calibration curve established with standard SA55 solutions of 100, 20, and 4 ng/mL and served as the internal reference in each assay. Among all 113 participants invited in the first round of sampling in September 2023, 22 were resampled and examined again in March 2024. All of them experienced a flu-like syndrome during the six months, with several confirmed to have SARS-CoV-2 infection.

The IgG binding kinetics assays for blood samples were also carried out using a similar protocol mentioned previously (Figure S4B). To evaluate the binding kinetics of the antibodies, the sample incubation times were set to 2, 4, and 8 min (Figure 5).

Design and Construction of the Engineered Proteins Used in RIVIA 2.0

For RIVIA 2.0, a recombinant hACE2 was designed, expressed, and provided by Sino Biological Inc., containing an active hACE2 ECD, a human IgG-Fc domain, and a spacer in between (hACE2-hFc; Beijing, China; Cat#10108-H02H). The IgG-Fc domain was primarily used in protein purification but also served as the anchor for immobilization on TOI microfluidic immunoreactors. The hACE2-hFc serves as the mock receptor for SARS-CoV-2 S proteins in the RIVIA assays (Figures S8 and S6).

Additionally, a specially designed S-ECD of WT and XBB.1.16 strains were also expressed and purified by Sino Biological Inc. (Beijing, China). Each engineered monomer contains an S-ECD, a T4 trimerization domain, an Avi-tag, and a biotin on the N-terminal. The Avi-tag biotinylation was designed to provide an orientation-specific labeling that can maximize the binding and signaling efficiency. Due to the presence of the T4 trimerization domain, the homotrimer of the engineered S-ECD will form automatically. AlphaFold3 simulations for these two proteins can be found in Figure S8, and an illustrational comparison between the biotinylated S-ECD trimers used in our original RIVIA and RIVIA 2.0 can be found in Figure S9.

Optimization of RIVIA 2.0

For the RIVIA 2.0 assay, the recombinant hACE2 was first immobilized on the inner surface of the TOI immunoreactors through 1-h physical adsorption at 15 μg/mL. After the two consecutive blocking steps, the sample and S-ECD mixture solution were drawn into the TOI immunoreactors. The final concentration of the engineered AVI-tag biotinylated S-ECD homotrimer was 10 ng/mL. This concentration was chosen to produce a stable and strong chemiluminescence signal under the same conditions in the absence of antibodies or nanobodies. The optimization of S-ECD homotrimer concentration can be found in Figure S10. For CL signal measurement, a 3000×-diluted SA poly-HRP solution was used for the visualization of the biotinylated S-ECD attached to the reactor surface.

Performance Evaluation of the RIVIA 2.0

To construct the calibration curves of RIVIA 2.0, various concentrations of SA55, SA58, and D006 were prepared through serial dilutions. The fingertip blood samples collected from volunteers were tested at 50× dilution and incubated for 10 min in the immunoreactors. For each set of assays (12 reactors), one of the immunoreactors was used as the positive control (1 μg/mL SA55), and two were used as the negative controls (1% casein in PBS). The CVs of RIVIA 2.0 were also obtained with 6 repeated tests of 1-μg/mL SA55 and SA58 as mock samples.

Conventional Pseudovirus Neutralization Test

To generate the pseudovirus, the S protein gene of the SARS-CoV-2 variant was codon optimized and inserted into the pcDNA3.1 vector. The vector containing the S protein gene was co-transfected with the G*ΔG-VSV virus (Kerafast, California, USA; Cat#EH1020-PM) into 293T cells (ATCC, Virginia, USA; Cat#CRL-3216). After cell culturing, the supernatant was collected by centrifugation, filtered, and aliquoted for storage.

In a 96-well cell culture plate, the serum to be tested was diluted in a gradient using a Dulbecco's modified Eagle medium (DMEM) medium (Hyclone, Utah, USA; Cat#SH30243.01). The pseudovirus was then added, and the mixture was incubated at 37 °C for 1 h. Huh-7 cells (Japanese Collection of Research Bioresources, Osaka, Japan; Cat#0403) were digested into a single-cell suspension, added to the wells, and incubated at 37 °C with 5% CO_2 for approximately 24 h. Half of the supernatant was then discarded, and Bright-Lite Luciferase Assay Substrate (lyophilized) mixed with Bright-Lite Luciferase Assay Buffer (Vazyme, Jiangsu, China; Cat#DD1209-03-AB) was added. The plate was then kept in the dark to allow the reaction to proceed. The cell lysate was transferred to a white 96-well detection plate, and luminescence intensity was measured using a microplate spectrophotometer. Dose-response curves were fitted using a four-parameter logistic regression model to calculate the half-maximal inhibitory concentration (IC_{50}).

Principal Component Analysis and Phylogenetic Inference of RBDs

The pretrained protein language model ESM-MSA-1b [74,75] was downloaded from https://dl.fbaipublicfiles.com/fair-esm/models/esm_msa1b_t12_100M_UR50S.pt shown on the ESM GitHub page (https://github.com/facebookresearch/esm). Intact S-protein sequences were aligned by MAFFT v7.505 [76] using the LINSi algorithm. Selected SARS-CoV-2 RBD domains (SARS, WT, Alpha, Beta, Gamma, Delta, D614G, Omicron

BA1, BA2, BA3, BA.4/5, XBB.1.5., XBB.1, EG.5, JN.1, and BA2.86) were extracted from the alignment, and each sequence with gaps was encoded by ESM alphabet. Start token "<cls>" and end token "<eos>" were attached to the beginning and the end of each encoded sequence. Each encoded sequence was then input into ESM-MSA-1b to get a local embedding with dimension $L \times 768$, in which L indicates the sequence length. The local embeddings of all RBD sequences were flattened and stacked as one matrix. Principal component analysis (PCA) dimension reduction was conducted by the sklearn.decomposition. PCA.fit_transform function implemented in Scikit-learn 1.1.1 [77], with default parameters. Phylogeny inference was conducted by IQ-TREE 2.2.565 [78] under default settings, based on RBD domain sequence alignment. Tree visualization was supported by iTOL 6.9.1 [79] (Figure S11).

ACKNOWLEDGEMENTS

This study was supported by the Outstanding Young Innovator Fund, Shenzhen Institute of Advanced Technology, Chinese Academy of Sciences (to X.T.), and the State Key Laboratory of Biomedical Imaging Science and System; Shenzhen Basic Research Project of Natural Science Foundation (JCYJ20230808105701004 to Y.C.), Shenzhen Science and Technology Innovations Committee (JSGGZD20220822095200001 to H.Y.), National Science Foundation of China (32270937 to F.Y.), Ministry of Science and Technology of China (2021D0102 to Y.C.), Guangdong Basic and Applied Basic Research Foundation (2025A1515012136 to H.L.), and Medicine Plus Program of Shenzhen University (2024YG015 to Y.C.).

The authors thank Mr. Yangang Huang from Beijing 4.0 Industrial Technology Co., Ltd. for the support in microfluidic immunoreactor fabrication. The authors thank Dr. Heng Zou from the Second Affiliated Hospital of the Chongqing Medical University for providing pre-COVID samples. The authors thank Miss Ziwei Zhu for the thoughtful discussions and kind support during the figure preparation. The authors sincerely thank all volunteers for their kind support in this research.

DECLARATION OF COMPETING INTERESTS

The authors declare that they have no known competing financial interests or personal relationships that could have appeared to influence the work reported in this paper.

ETHICS APPROVAL

The research protocol and the collection of human blood samples, including fingertip blood, fingertip serum, venous blood, and venous serum were approved by the Institutional Review Broad (IRB) of Shenzhen Institute of Advanced Science, Chinese Academy of Science (SIAT-IRB-230715-H0667). All participating volunteers signed the informed consent form during the sample collection visit.

AUTHOR CONTRIBUTIONS

Xiaotian Tan: conceptualization, funding acquisition, project administration, supervision, methodology, resources, investigation, validation, visualization, writing – original draft, writing – review & editing. **Yujuan Chai:** conceptualization, funding acquisition, supervision, methodology, investigation, writing – original draft, writing – review & editing. **Ruihan Li:** conceptualization, methodology, investigation, validation, data curation, visualization, writing – original draft. **Binmao Zhang:** methodology, investigation, validation, data curation, visualization, writing – original draft. **Hao Li:** conceptualization, project administration, supervision, methodology, investigation, validation, writing – original draft, writing – review & editing. **Jie Zhang:** conceptualization, funding acquisition, supervision, resources, writing – review & editing. **Tianen Zhu:** investigation, validation. **Weishu Wu:** data curation. **Lixiang An:** methodology, investigation, validation. **Shi Hu:** investigation, validation. **Bin Yang:** methodology, resources. **Li Wang:** methodology, resources. **Zhenqiu Cao:** data curation, visualization. **Hongjiu Zhang:** data curation, visualization. **Peng Wang:** validation. **Lingling Yu:** validation. **Shan Yin:** resources. **Xingyu Li:** resources. **Fei Shao:** validation. **Jianheng Huang:** investigation. **Jinze Li:** investigation. **Fan Yang:** conceptualization, funding acquisition, writing – review & editing. **Chao Zhao:** conceptualization, writing – review & editing. **Jiajia Guo:** conceptualization, writing – review & editing. **Lin Zeng:** investigation. **Dong Liang:** funding acquisition, supervision. **Zhengting Zou:** conceptualization, validation, data curation, writing – review & editing. **Hairong Zheng:** funding acquisition, supervision. **Xudong Fan:** conceptualization, supervision, writing – original draft, writing – review & editing. **Liangzhi Xie:** supervision, resources. **Yunlong Cao:** conceptualization, supervision, resources, validation, writing – original draft, writing – review & editing. **Hui Yang:** conceptualization, funding acquisition, project administration, supervision, methodology, resources, investigation, writing – original draft, writing – review & editing.

SUPPLEMENTARY DATA

Supplementary data to this article can be found online at https://doi.org/10.1016/j.hlife.2025.04.005.

REFERENCES

[1] Sachs JD, Karim SSA, Aknin L, Allen J, Brosbøl K, Colombo F, et al. The *Lancet* Commission on lessons for the future from the COVID-19 pandemic. *Lancet* 2022;400:1224–80.
[2] Chow EJ, Uyeki TM, Chu HY. The effects of the COVID-19 pandemic on community respiratory virus activity. *Nat Rev Microbiol* 2023;21:195–210.
[3] Su C, He J, Xie Y, Hu Y, Li X, Qiao S, et al. Enabling the immune escaped etesevimab fully-armed against SARS-CoV-2 Omicron subvariants including KP.2. *hLife* 2025;3:132–45.
[4] Gao L, Yang H, He P, Yang S, Li W, Li F, et al. Safety and immunogenicity of COVID-19 vaccine ZF2001 in Chinese aged 60 years and older. *hLife* 2024;2:257–61.
[5] Raveendran AV, Jayadevan R, Sashidharan S. Long COVID: An overview. *Diabetes Metab Syndr* 2021;15:869–75.
[6] Menni C, Sudre CH, Steves CJ, Ourselin S, Spector TD. Quantifying additional COVID-19 symptoms will save lives. *Lancet* 2020;395:e107–8.
[7] Garcia-Beltran WF, Lam EC, Astudillo MG, Yang D, Miller TE, Feldman J, et al. COVID-19-neutralizing antibodies predict disease severity and survival. *Cell* 2021;184:476–488.e11.
[8] Shi R, Shan C, Duan X, Chen Z, Liu P, Song J, et al. A human neutralizing antibody targets the receptor-binding site of SARS-CoV-2. *Nature* 2020;584:120–4.
[9] Wu Y, Wang F, Shen C, Peng W, Li D, Zhao C, et al. A noncompeting pair of human neutralizing antibodies block COVID-19 virus binding to its receptor ACE2. *Science* 2020;368:1274–8.
[10] Li G, Hilgenfeld R, Whitley R, De Clercq E. Therapeutic strategies for COVID-19: Progress and lessons learned. *Nat Rev Drug Discov* 2023;22:449–75.
[11] Cao Y, Jian F, Wang J, Yu Y, Song W, Yisimayi A, et al. Imprinted SARS-CoV-2 humoral immunity induces convergent Omicron RBD evolution. *Nature* 2023;614:521–9.
[12] Dhama K, Nainu F, Frediansyah A, Yatoo MI, Mohapatra RK, Chakraborty S, et al. Global emerging Omicron variant of SARS-CoV-2: Impacts, challenges and strategies. *J Infect Public Health* 2023;16:4–14.

[13] Kang H, Jung J, Ko GY, Lee J, Oh EJ. Evaluation of long-term adaptive immune responses specific to SARS-CoV-2: Effect of various vaccination and Omicron exposure. *Vaccines* 2024;12:301.

[14] Clemente-Suárez VJ, Hormeño-Holgado A, Jiménez M, Benitez-Agudelo JC, Navarro-Jiménez E, Perez-Palencia N, et al. Dynamics of population immunity due to the herd effect in the COVID-19 pandemic. *Vaccines (Basel)* 2020;8:236.

[15] Wang Q, Zhang Y, Wu L, Niu S, Song C, Zhang Z, et al. Structural and functional basis of SARS-CoV-2 entry by using human ACE2. *Cell* 2020;181:894–904.e9.

[16] Zeng B, Gao L, Zhou Q, Yu K, Sun F. Effectiveness of COVID-19 vaccines against SARS-CoV-2 variants of concern: A systematic review and meta-analysis. *BMC Med* 2022;20:200.

[17] Xu K, Gao P, Liu S, Lu S, Lei W, Zheng T, et al. Protective prototype-Beta and Delta-Omicron chimeric RBD-dimer vaccines against SARS-CoV-2. *Cell* 2022;185:2265–2278.e14.

[18] Hu X, Qian M, Cheng B, Cheung YK. Personalized policy learning using longitudinal mobile health data. *J Am Stat Assoc* 2021;116:410–20.

[19] Kim SJ, Yao Z, Marsh MC, Eckert DM, Kay MS, Lyakisheva A, et al. Homogeneous surrogate virus neutralization assay to rapidly assess neutralization activity of anti-SARS-CoV-2 antibodies. *Nat Commun* 2022;13:3716.

[20] Deeks JJ, Dinnes J, Takwoingi Y, Davenport C, Spijker R, Taylor-Phillips S, et al. Antibody tests for identification of current and past infection with SARS-CoV-2. *Cochrane Database Syst Rev* 2020;6:CD013652.

[21] Su H, Zhang J, Yi Z, Khan S, Peng M, Ye L, et al. A human monoclonal antibody neutralizes SARS-CoV-2 Omicron variants by targeting the upstream region of spike protein HR2 motif. *hLife* 2024;2:126–40.

[22] Tan CW, Zhu F, Chia WN, Young BE, Yeoh AYY, Althaus T, et al. Distinctive serotypes of SARS-related coronaviruses defined by convalescent sera from unvaccinated individuals. *hLife* 2023;1:26–34.

[23] Pickering S, Betancor G, Galão RP, Merrick B, Signell AW, Wilson HD, et al. Comparative assessment of multiple COVID-19 serological technologies supports continued evaluation of point-of-care lateral flow assays in hospital and community healthcare settings. *PLoS Pathog* 2020;16:e1008817.

[24] Kerr C, Dunne J, Hughes G, Cox F, Healy M, Holmes P, et al. A comparison of the performance of SARS-CoV-2 antibody assays in healthcare workers with COVID-19. *Ir Med J* 2021;114:414.

[25] Colombini A, Viganò M, Tomaiuolo R, Di Resta C, Corea F, Sabetta E, et al. Exploratory assessment of serological tests to determine antibody titer against SARS-CoV-2: Appropriateness and limits. *J Clin Lab Anal* 2022;36:e24363.

[26] Schmidt F, Weisblum Y, Muecksch F, Hoffmann HH, Michailidis E, Lorenzi JCC, et al. Measuring SARS-CoV-2 neutralizing antibody activity using pseudotyped and chimeric viruses. *J Exp Med* 2020;217:e20201181.

[27] Zedan HT, Yassine HM, Al-Sadeq DW, Liu N, Qotba H, Nicolai E, et al. Evaluation of commercially available fully automated and ELISA-based assays for detecting anti-SARS-CoV-2 neutralizing antibodies. *Sci Rep* 2022;12:19020.

[28] Cheng J, Fu Y, Guo J, Guo J. A low-cost paper-based blood urea nitrogen optical biosensor for renal surveillance in fingertip blood. *Sens Actuators B Chem* 2023;387:133795.

[29] Senel M. Electrochemistry test strip as platform for *in situ* detection of blood levels of antipsychotic clozapine in finger-pricked sample volume. *Biosensors (Basel)* 2023;13:346.

[30] Cheah E, Tran DP, Amen MT, Arrua RD, Hilder EF, Thierry B. Integrated platform addressing the finger-prick blood processing challenges of point-of-care electrical biomarker testing. *Anal Chem* 2022;94:1256–63.

[31] Swank Z, Michielin G, Yip HM, Cohen P, Andrey DO, Vuilleumier N, et al. A high-throughput microfluidic nanoimmunoassay for detecting anti-SARS-CoV-2 antibodies in serum or ultralow-volume blood samples. *Proc Natl Acad Sci USA* 2021;118:e2025289118.

[32] Debnath N, Live LS, Poudineh M. A microfluidic plasma separation device combined with a surface plasmon resonance biosensor for biomarker detection in whole blood. *Lab Chip* 2023;23:572–9.

[33] Wang X, He X, He Z, Hou L, Ge C, Wang L, et al. Detection of prostate specific antigen in whole blood by microfluidic chip integrated with dielectrophoretic separation and electrochemical sensing. *Biosens Bioelectron* 2022;204:114057.

[34] Tan X, Khaing Oo MK, Gong Y, Li Y, Zhu H, Fan X. Glass capillary based microfluidic ELISA for rapid diagnostics. *Analyst* 2017;142:2378–85.

[35] Tan X, David A, Day J, Tang H, Dixon ER, Zhu H, et al. Rapid mouse follicle stimulating hormone quantification and estrus cycle analysis using an automated microfluidic chemiluminescent ELISA system. *ACS Sens* 2018;3:2327–34.

[36] Shamsi MH, Choi K, Ng AH, Wheeler AR. A digital microfluidic electrochemical immunoassay. *Lab Chip* 2014;14:547–54.

[37] Herr AE, Hatch AV, Throckmorton DJ, Tran HM, Brennan JS, Giannobile WV, et al. Microfluidic immunoassays as rapid saliva-based clinical diagnostics. *Proc Natl Acad Sci USA* 2007;104:5268–73.

[38] Campbell S, Anderson N, Babady E, Durant TJS, Fisher A, Moore N. Centralized *vs* decentralized molecular infectious disease testing. *Clin Chem* 2021;67:713–9.

[39] Arboleda VA, Garner OB. Ensuring the quality of point-of-care testing in a large and decentralized ambulatory care setting. *Am J Clin Pathol* 2017;148:336–44.

[40] Ao D, He X, Hong W, Wei X. The rapid rise of SARS-CoV-2 Omicron subvariants with immune evasion properties: XBB.1.5 and BQ.1.1 subvariants. *MedComm* 2023;4:e239.

[41] Feng Y, Su Q, Li L, He X, Niu P, Guo X, et al. Genomic surveillance for SARS-CoV-2 variants: Dominance of XBB replacement — China, January–June 2023. *China CDC Wkly* 2024;6:324–31.

[42] Velavan TP, Ntoumi F, Kremsner PG, Lee SS, Meyer CG. Emergence and geographic dominance of Omicron subvariants XBB/XBB.1.5 and BF.7 – the public health challenges. *Int J Infect Dis* 2023;128:307–9.

[43] He X, Aid M, Chandrashekar A, Yu J, McMahan K, Wegmann F, et al. A homologous or variant booster vaccine after Ad26.COV2.S immunization enhances SARS-CoV-2-specific immune responses in rhesus macaques. *Sci Transl Med* 2022;14:eabm4996.

[44] Bates TA, Leier HC, McBride SK, Schoen D, Lyski ZL, Lee DX, et al. An extended interval between vaccination and infection enhances hybrid immunity against SARS-CoV-2 variants. *JCI Insight* 2023;8:e165265.

[45] Lyu Y, Zhang B, Chai Y, Zhang J, Wang L, Xiao Y, et al. A quantitative first passage time model for tubular microfluidic immunoassays. *ACS Sens* 2025;10:1387–97.

[46] Zhang B, Xu Y, Huang Z, Li R, Zhu T, Liang S, et al. Consolidated microscale interferon-γ release assay with tip optofluidic immunoassay for dynamic parallel diagnosis of tuberculosis infection. *Anal Chem* 2025;97:2863–72.

[47] Cao Y, Wang J, Jian F, Xiao T, Song W, Yisimayi A, et al. Omicron escapes the majority of existing SARS-CoV-2 neutralizing antibodies. *Nature* 2022;602:657–63.

[48] Cao Y, Su B, Guo X, Sun W, Deng Y, Bao L, et al. Potent neutralizing antibodies against SARS-CoV-2 identified by high-throughput single-cell sequencing of convalescent patients' B cells. *Cell* 2020;182:73–84.e16.

[49] Wu W, Tan X, Zupancic J, Schardt JS, Desai AA, Smith MD, et al. Rapid and quantitative *in vitro* evaluation of SARS-CoV-2 neutralizing antibodies and nanobodies. *Anal Chem* 2022;94:4504–12.

[50] Pan Y, Wang L, Feng Z, Xu H, Li F, Shen Y, et al. Characterisation of SARS-CoV-2 variants in Beijing during 2022: An epidemiological and phylogenetic analysis. *Lancet* 2023;401:664–72.

[51] Wang C, Han B, Zhao T, Liu H, Liu B, Chen L, et al. Vaccination willingness, vaccine hesitancy, and estimated coverage at the first round of COVID-19 vaccination in China: A national cross-sectional study. *Vaccine* 2021;39:2833–42.

[52] Tan X, Krel M, Dolgov E, Park S, Li X, Wu W, et al. Rapid and quantitative detection of SARS-CoV-2 specific IgG for convalescent serum evaluation. *Biosens Bioelectron* 2020;169:112572.

[53] Jia S, Yin Z, Pan H, Wang F, Liu X, Wang Q, et al. Relative effectiveness of a heterologous booster dose with adenovirus type 5 vectored COVID-19 vaccine *versus* three doses of inactivated COVID-19 vaccine in adults during a nationwide outbreak of omicron predominance, in China: A retrospective, individually matched cohort-control study. *Emerg Microbes Infect* 2024;13:2332660.

[54] Meijers M, Ruchnewitz D, Eberhardt J, Łuksza M, Lässig M. Population immunity predicts evolutionary trajectories of SARS-CoV-2. *Cell* 2023;186:5151–5164.e13.

[55] Cao Y, Yisimayi A, Jian F, Song W, Xiao T, Wang L, et al. BA.2.12.1, BA.4 and BA.5 escape antibodies elicited by Omicron infection. *Nature* 2022;608:593–602.

[56] Yue C, Song W, Wang L, Jian F, Chen X, Gao F, et al. ACE2 binding and antibody evasion in enhanced transmissibility of XBB.1.5. *Lancet Infect Dis* 2023;23:278–80.

[57] Liu Y, Wang Z, Zhuang X, Zhang S, Chen Z, Zou Y, et al. Inactivated vaccine-elicited potent antibodies can broadly neutralize SARS-CoV-2 circulating variants. *Nat Commun* 2023;14:2179.

[58] Wang K, Jia Z, Bao L, Wang L, Cao L, Chi H, et al. Memory B cell repertoire from triple vaccinees against diverse SARS-CoV-2 variants. *Nature* 2022;603:919–25.

[59] Tan CW, Chia WN, Qin X, Liu P, Chen MIC, Tiu C, et al. A SARS-CoV-2 surrogate virus neutralization test based on antibody-mediated blockage of ACE2–spike protein–protein interaction. *Nat Biotechnol* 2020;38:1073–8.

[60] Devasenapathy N, Ye Z, Loeb M, Fang F, Najafabadi BT, Xiao Y, et al. Efficacy and safety of convalescent plasma for severe COVID-19 based on evidence in other severe respiratory viral infections: A systematic review and meta-analysis. *CMAJ* 2020;192:E745–55.

[61] Yewdell JW. Antigenic drift: Understanding COVID-19. *Immunity* 2021;54:2681–7.

[62] Koyama T, Weeraratne D, Snowdon JL, Parida L. Emergence of drift variants that may affect COVID-19 vaccine development and antibody treatment. *Pathogens* 2020;9:324.

[63] Bai Y, Peng Z, Wei F, Jin Z, Wang J, Xu X, et al. Study on the COVID-19 epidemic in mainland China between November 2022 and January 2023, with prediction of its tendency. *J Biosaf Biosecur* 2023;5:39–44.
[64] Kenny G, O'Reilly S, Wrigley Kelly N, Negi R, Gaillard C, Alalwan D, et al. Distinct receptor binding domain IgG thresholds predict protective host immunity across SARS-CoV-2 variants and time. *Nat Commun* 2023;14:7015.
[65] Yisimayi A, Song W, Wang J, Jian F, Yu Y, Chen X, et al. Repeated Omicron exposures override ancestral SARS-CoV-2 immune imprinting. *Nature* 2024;625:148–56.
[66] Huang CQ, Vishwanath S, Carnell GW, Chan ACY, Heeney JL. Immune imprinting and next-generation coronavirus vaccines. *Nat Microbiol* 2023;8:1971–85.
[67] Röltgen K, Nielsen SCA, Silva O, Younes SF, Zaslavsky M, Costales C, et al. Immune imprinting, breadth of variant recognition, and germinal center response in human SARS-CoV-2 infection and vaccination. *Cell* 2022;185:1025–1040.e14.
[68] Yang S, Yu Y, Xu Y, Jian F, Song W, Yisimayi A, et al. Fast evolution of SARS-CoV-2 BA.2.86 to JN.1 under heavy immune pressure. *Lancet Infect Dis* 2024;24:e70–2.
[69] Alhamid G, Tombuloglu H, Rabaan AA, Al-Suhaimi E. SARS-CoV-2 detection methods: A comprehensive review. *Saudi J Biol Sci* 2022;29:103465.
[70] Tan X, Li R, Yang H. Antibody probes in biomolecular sensing: Transitioning from carbon-based computing to silicon-based computing. *Synth Biol J* 2024;5:1–9 (in Chinese).
[71] Ye Z, Bonam SR, McKay LGA, Plante JA, Walker J, Zhao Y, et al. Monovalent SARS-COV-2 mRNA vaccine using optimal UTRs and LNPs is highly immunogenic and broadly protective against Omicron variants. *Proc Natl Acad Sci USA* 2023;120:e2311752120.
[72] Cao Y, Jian F, Zhang Z, Yisimayi A, Hao X, Bao L, et al. Rational identification of potent and broad sarbecovirus-neutralizing antibody cocktails from SARS convalescents. *Cell Rep* 2022;41:111845.
[73] Chai Y, Li Q, Wang Y, Niu B, Chen H, Fan T, et al. Cortisol dysregulation in anxiety infertile women and the influence on IVF treatment outcome. *Front Endocrinol* 2023;14:1107765.
[74] Rives A, Meier J, Sercu T, Goyal S, Lin Z, Liu J, et al. Biological structure and function emerge from scaling unsupervised learning to 250 million protein sequences. *Proc Natl Acad Sci USA* 2021;118:e2016239118.
[75] Rao RM, Liu J, Verkuil R, Meier J, Canny J, Abbeel P, et al. MSA transformer. *Proc Mach Learn Res* 2021;139:8844–56.
[76] Katoh K, Standley DM. MAFFT multiple sequence alignment software version 7: Improvements in performance and usability. *Mol Biol Evol* 2013;30:772–80.
[77] Buitinck L, Louppe G, Blondel M, Pedregosa F, Mueller A, Grisel O, et al. API design for machine learning software: Experiences from the scikit-learn project. arXiv (2013). https://doi.org/10.48550/arXiv.1309.0238.
[78] Minh BQ, Schmidt HA, Chernomor O, Schrempf D, Woodhams MD, von Haeseler A, et al. IQ-TREE 2: New models and efficient methods for phylogenetic inference in the genomic era. *Mol Biol Evol* 2020;37:1530–4.
[79] Letunic I, Bork P. Interactive Tree of Life (iTOL) v6: Recent updates to the phylogenetic tree display and annotation tool. *Nucleic Acids Res* 2024;52:W78–82.